hydroxyethylpiperazine -N'- 2-ethanesulfonic acid (HEPES), 2 mM glutamine and 100μg/ml ampicillin (Sigma Chemical Co., St. Louis, MO). One half ml was seeded into 24 well tissue culture plates (Corning) containing 13 mm LUX coverslips (Nunc Thermanox coverslips, NalgeNunc, Thermo Scientific, Rochester, NY). After 20 hr adherence of the cells, macrophage monolayers were obtained after washing non-adherant cells from the coverslip with Hanks Balanced Salt Solution (HBSS, Sigma) leaving approximately 1×10^6 macrophages adhered per coverslip.

Human macrophage culture: Human peripheral blood was obtained under informed consent from healthy individuals. Peripheral blood mononuclear cells (PBMC) were isolated using Ficoll-Paque Plus (GE Healthcare Life Sciences, Buckinghamshire, HP7 9NA, UK) gradient centrifugation[10]. The cells were suspended in AIM-V medium (Gibco BRL, Invitrogen Corp., Carlsbad, CA) and 1×10^6 PBMC were cultured in a well of a 24-well tissue culture plate (Falcon, Becton Dickinson Labware, Becton Dickinson and Company, Franklin Lakes) containing 13 mm LUX coverslips at 37°C in a 5%-CO_2 incubator for adherence of monocytes. After 1 hr incubation, the coverslips were washed with HBSS to remove non-adherent cells. The monocytes on the coverslips were cultured in a new 24-well plate containing RPMI1640 medium (Sigma) supplemented with 20% FBS (Whittaker Co., Walkersville, MD), 25mM HEPES, 2mM L-glutamine and 100μg/ml ampicillin in the presence of 10 ng/ml of human M-CSF (R&D Systems, Minneapolis, MN) or 40 ng/ml of GM-CSF (R&D Systems). After 7 days, the M-CSF-conditioned macrophages (M-macrophages) and the GM-CSF-conditioned macrophages (GM-macrophages) were used for infection with *M.leprae*.

Infection of macrophages with *M.leprae*: Purified mouse macrophage monolayers were infected with fresh *M.leprae* suspended in 0.5 ml medium per well. After 4 hr incubation for mouse macrophages and 20 hr incubation for human macrophages, non-phagocytosed bacilli were removed by washing and the cultures were incubated in 1.0 ml media supplemented with the appropriate cytokine in 5% CO_2 at the appropriate experimental temperatures[9]. Media were changed and cytokines were replenished at 5 days interval.

Radiorespirometry: The macrophages were lysed with 0.1 N NaOH to release the phagocytosed *M.leprae*, and the viability of the bacilli was determined by evaluating the oxidation of ^{14}C-palmitic acid to $^{14}CO_2$ by radiorespirometry as described previously [11]. Total isotope release was usually analyzed after one week of incubation at 31°C [9].

Staining of *M.leprae*-infected macrophages: Coverslips of *M.leprae*-infected adherent macrophages were prefixed with absolute methanol and acid-fast stained. The specimens were observed under Nikon Optiphot light microscopy.

Results

Viability of *M.leprae* in mouse macrophages cultured *in vitro*: Mouse peritoneal resident macrophages (1×10^6 cells per well) were incubated with freshly harvested *M.leprae* (multiplicity of infection (MOI), 5:1 or 10:1) for 4 hr to allow phagocytosis. Non-phagocytosed bacilli were washed off and the culture of the macrophages continued for up to 14 days. Viability (metabolic activity) of *M.leprae* in macrophages was assessed by radiorespirometry. As shown in Fig. 1, the viability of the bacilli was gradually decreased in macrophages cultured at 35°C. In contrast, the viability was significantly lost, if the macrophages were cultured at 37°C. Next, the mouse peritoneal

resident macrophages were incubated with 3 doses of *M.leprae* (MOI, 1:1, 4:1 and 10:1) for 4 hr to allow phagocytosis, and the culture continued for longer periods up to 21 days. Viability of *M.leprae* in macrophages was assessed at 7 day intervals. As shown in Fig. 2, in each dose of *M.leprae* infection, decrease in viability was significant after 21 days.

Effects of cytokines on viability of *M.leprae* in mouse macrophages: Supplementation of IL-10 to the infected macrophage culture was

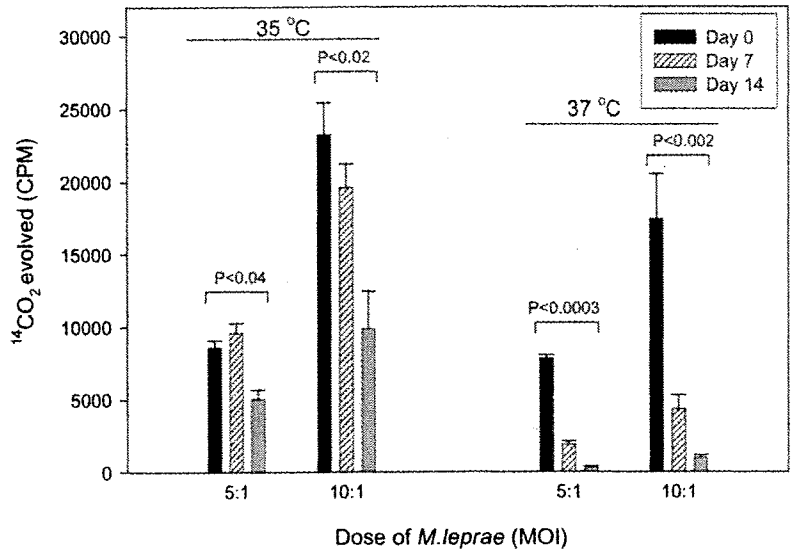

Fig.1. Viability of *M.leprae* in mouse macrophages cultured *in vitro*. Mouse peritoneal resident macrophages were incubated with 5×10^6 or 1×10^7 per well of *M.leprae* (MOI, 5:1 or 10:1), for 4 hr at 37°C to allow phagocytosis. Non-phagocytosed bacilli were washed off and the culture of the macrophages continued up to 14 days at 35°C or 37°C. The cells were lysed to obtain *M.leprae* and metabolism of the bacilli was assessed by radiorespirometry.

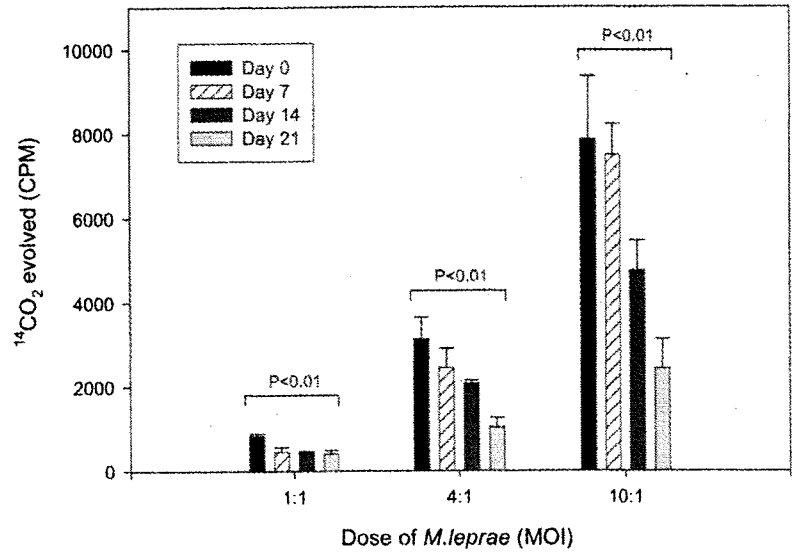

Fig.2. Viability of *M.leprae* in mouse macrophages cultured *in vitro*. Mouse peritoneal resident macrophages were incubated with 3 doses, 1×10^6, 4×10^6 and 1×10^7 per well of *M.leprae* (MOI, 1:1, 4:1 and 10:1) at 35°C for 4 hr to allow phagocytosis, and the culture continued at 35°C for longer periods up to 21 days. The cells were lysed to obtain *M.leprae* and metabolism of the bacilli was assessed by radiorespirometry.

clearly associated with sustained viability of intracellular *M.leprae* cultured at 35°C (Fig.3). In the presence of 3 U/ml of IL-10, *M.leprae* maintained their viability, whereas viability was steadily lost without IL-10. We also examined the effect of TGF-β, another suppressive cytokine for macrophage activation, on the viablility of the bacilli. To the contrary, supplementation of TGF-β

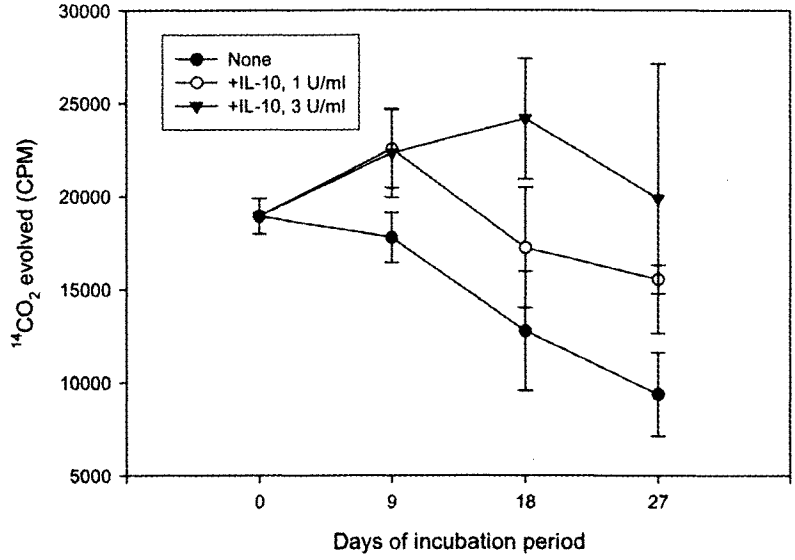

Fig.3. Effect of IL-10 on *M.leprae* survival in mouse macrophages. Mouse peritoneal resident macrophages were incubated with 1×10^7 per well of *M.leprae* (MOI, 10:1) at 35°C for 4 hr to allow phagocytosis, and the culture continued at 35°C for 9, 18 and 27 days. The cells were lysed to obtain *M.leprae* and metabolism of the bacilli was assessed by radiorespirometry.

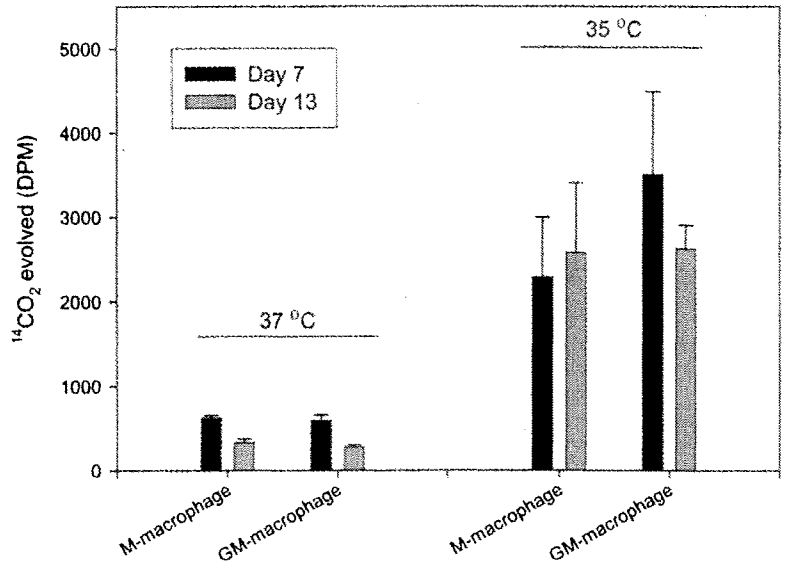

Fig.4. Viability of *M.leprae* in human macrophages cultured *in vitro*. Human M- or GM-macrophages were incubated with *M.leprae* (MOI, 50:1) for 20 hr either at 35°C or 37°C for infection and incubated at the same temperatures for indicated periods. By observation of the acid fast-stained cells under light microscopy, no difference was recognized in the number of *M.leprae* phagocytosed by macrophage cultured between at 35°C and at 37°C. So the viability at day 0 is considered equal. After 7 days and 13 days incubation period, the cells were lysed to obtain *M.leprae* and metabolism of the bacilli was assessed by radiorespirometry (dpm: disintegrations per minute).

significantly decreased the viability of *M.leprae*, when incubated for longer than 28 days post infection (Table 1).

Viability of *M.leprae* in human macrophages cultured *in vitro*: Human macrophages were obtained by culturing monocytes in the presence of either M-CSF or GM-CSF for 7 days. These macrophages (1×10^5 cells per well) were incubated with *M.leprae* (MOI, 50:1) for 20 hr either at 35°C or 37°C for infection and incubated again at the same temperatures. By observation of the acid fast-stained cells under light microscopy,

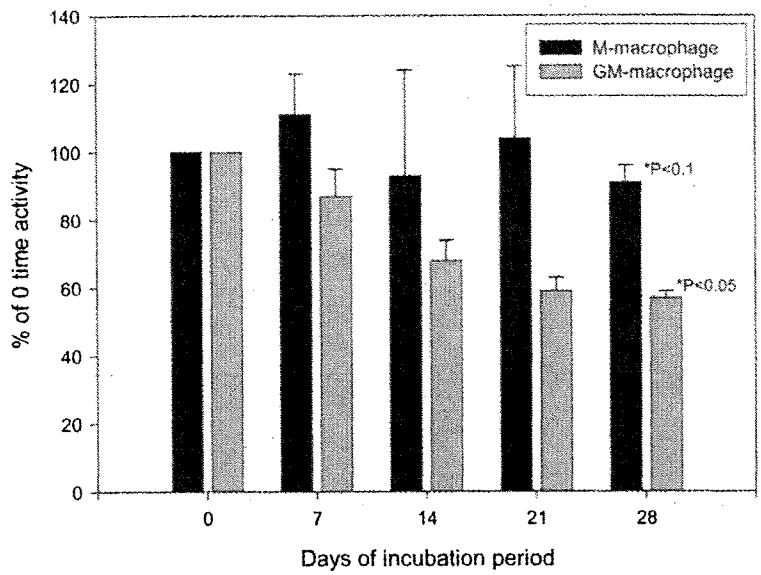

Fig.5. Viability of *M.leprae* in human macrophages cultured *in vitro*. Human M- or GM-macrophages were infected with *M.leprae* (MOI, 50:1) for 20 hr at 35°C and incubated again at 35°C for indicated periods. The cells were lysed to obtain *M.leprae* and metabolism of the bacilli was assessed by radiorespirometry. The results at day 7, 14, 21 and 28 are expressed as percentages of *M.leprae* metabolic activity at time 0. Radiorespirometry data obtained from *M.leprae* in M-macrophages at time 0 was 5,932±399 and those in GM-macrophages was 3,084±78. *P values calculated in comparison to day 0 viability.

Table 1. Effect of TGF-β on survival of *M.leprae* in mouse macrophages cultured at 35°C[a]

Experiment 1

Days of incubation period	At time 0	7	14	28
Medium only	5,222±936[b]	2,774±295	3,086±425	2,828±1,815
+TGF-β		2,919±535	3,119±1,339	1,973±126

Experiment 2

Days of incubation period	At time 0	14	28	49
Medium only	26,791±1,428	19,103±621	7,420±2,986	5,713±1,144
+TGF-β		14,306±2,240	3,728±410	1,594±317

[a]Mouse peritoneal resident macrophages were incubated with *M.leprae* (MOI, 1:10) for 4 hr to allow phagocytosis, and the culture continued for indicated periods. The cells were lysed to obtain *M.leprae* and metabolism of the bacilli was assessed by radiorespirometry.
[b]Radiorespirometry data, cpm.
Dose of TGF-β, 500pg/ml.
N.D., not determined.

no difference was recognized in the number of *M.leprae* phagocytosed by macrophage cultured at 35°C and at 37°C (data not shown). Viability of *M.leprae* was assessed after 7 and 13 days. The results clearly showed that the viability of *M.leprae* incubated at 35°C was maintained, whereas the viability was lost if cultured at 37°C (Fig. 4). Next, *M.leprae*-infected human M- and GM-macrophages were cultured for prolonged periods at 35°C. Viability was sustained well for 4 weeks in human macrophages, especially in M-macrophages (Fig. 5).

Discussion

In vivo M.leprae is able to enter and survive in a wide variety of tissues and cell types[12]. The preferred host cell for the leprosy bacillus appears to be the macrophages and a number of unsuccessful attempts have been made to grow *M.leprae* in macrophages *in vitro*. For example, Sharp and Banerjee[13] employed macrophages from conventional mice and rats, *nu/nu* mice or *nu/nu* rats and armadillos. The *M.leprae* inocula were derived from 3 sources (human leproma, *nu/nu* mouse footpad and frozen infected armadillo tissue). Incubation temperature was varied from 31°C to 35°C and *M.leprae*-infected cells were maintained for up to 200 days. Fieldsteel and McIntosh [14] employed a range of rat, mouse and human tissue. The conclusion of these reports is that no significant multiplication of *M.leprae* occurred in any of the cells or tissues.

Previously, we reported that metabolically active *M.leprae* could be maintained in monolayer cultures of mouse peritoneal macrophages and that supplemental IL-10 bolstered *M.leprae* metabolism in the macrophages for as long as 8 weeks. In the cell culture system, temperature is an extremely important factor for growth and 31-33°C incubation temperature is more permissive than 37°C [5]. In the present study, we further observed that incubation of mouse macrophages infected with *M.leprae* at 35°C was also more growth permissive than at 37°C. We chose 35°C as the incubation temperature, and not 31°C, because the maintenance of the integrity of the macrophage monolayer was better at 35°C than at 31-33°C. Moreover, the monolayer of *M.leprae*-infected human macrophages at 31-33°C could not be maintained for longer than one week. We observed that maintenance of the monolayer was good at 35°C, and *M.leprae* at 35°C was also more growth permissive than those at 37°C in human macrophages (Fig. 4 and 5). Our starting inoculum of *M.leprae* was freshly obtained for each experiment from infected *nu/nu* mice. We also were able to rapidly quantify the metabolic activity of *M.leprae* using the radiorespirometry technique adapted by Franzblau [11]. This assay is accurate and highly sensitive with the results available in a short duration of 1 wk (compared to 6-12 months when titrated in mouse footpads). Radiorespirometry data correlates well with other *in vitro* systems [11] but, more importantly, the data correlated well with "viability" as observed in the mouse footpad system [12].

Various clinical evidence suggests that *M.leprae* prefer a growth temperature of less than 37°C [1]. In animal models, *M.leprae* multiplies in the mouse foot pad where the temperature is lower than the body temperature [2]. In addition, *Dasypus novemcinctus*, the nine-banded armadillo has a core temperature of ~33°C, which renders it permissive as a host for the leprosy bacillus [13]. Mononuclear phagocytes in virtually every organ of the natural or experimentally infected armadillo become heavily parasitized with propagating *M. leprae* [14]. Whether intracellular or extracellular, *M.leprae* clearly prefers temperatures cooler than

normal human body temperature [12], and 37°C appeared to be highly detrimental to *M.leprae* viability. The *in vitro* results obtained in the present study confirmed the preference of lower temperature (35°C) by *M.leprae* residing in human macrophages.

In this study, supplemental IL-10, but not TGF-β supported the metabolic activity of *M.leprae* in mouse macrophages for several weeks, similar to the results obtained previously [5]. In choosing TGF-β and IL-10 as the cytokines that might bolster the intracellular survival of *M.leprae,* we were attempting to down-regulate any innate ability of the normal macrophages to cope with the organism. TGF-β is produced by activated macrophages and other inflammatory cells and has a broad array of modulatory functions on the immune response. TGF-β has been shown to interfere with macrophage antimicrobial mechanisms including the generation of reactive oxygen intermediates [15] and reactive nitrogen intermediates [16], and has been shown to enhance the intracellular growth of *M.tuberculosis* in human monocytes [17]. However, in the present studies with mouse macrophages, exogenous TGF-β had no detectable effect on sustaining intracellular *M.leprae* viability, and in fact decreased the viability (Table 1). In contrast, supplementing media with IL-10 clearly affected the long term viability of *M.leprae* in mouse macrophages (Fig. 3). IL-10 is produced by T cells, B cells and macrophages [18, 19]. IL-10 has been shown to be a potent down-regulator of cell-mediated immunity to intracellular pathogens [20]. *In vivo*, endogenous IL-10 dampened the cell-mediated immune response to avirulent mycobacterial infection [4] and appeared to lead to loss of control of *M.tuberculosis* infection with widespread dissemination [21]. IL-10 functions in part at the level of the macrophage by attenuating iNOS mRNA expression, iNOS activity and, by inference, NO production [22]. In human macrophages, however, the viability of *M.leprae* was maintained for 4 weeks in the absence of IL-10 (Fig. 5), suggesting that human cells seem to be better hosts than mouse cells for *M.leprae* survival. Viability of *M.leprae* in M-macrophages seems to be maintained for a longer period (up to one month) than that in GM-macrophages (Fig. 5). One of the reasons for this may be due to the production of IL-10 by M-macrophages [23], although the mechanism by which IL-10 contributes to the maintenance and growth of *M.leprae* is unclear.

In conclusion, the present study showed that the metabolism, and presumably the viability, of *M.leprae* could be sustained under culture conditions at 35°C, which is also a moderate temperature necessary to maintain the integrity of macrophages.

Acknowledgments

The study was supported partly by a Health Science Research Grant of Emerging and Re-emerging Infectious Diseases, from the Ministry of Health, Labour and Welfare of Japan. We are also grateful to the Japanese Red Cross Society for kindly providing PBMCs from healthy donors.

References

1) Brand PW: Temperature variation and leprosy deformity. Int J Lepr 27:1-7, 1959.
2) Shepard CC: Temperature Optimum of *Mycobacterium leprae* in Mice. J Bacteriol 90:1271-1275, 1965.
3) Yamamura M, Uyemura KD, Aeans RJ, Weinberg K, Rea TH, Bloom.BR, Modlin RL: Defining protective response to pathgens: cytokine profiles in leprosy lesions. Science 254:277-282, 1991.

4) Sharma S, Bose M: Role of cytokines in immune response to pulmonary tuberculosis. Asian Pac J Allergy Immunol 19: 213-219, 2001.
5) Fukutomi Y, Matsuoka M, Minagawa F, Toratani S, McCormick G, Krahenbuhl J: Subversion of macrophage anti-microbial function bolsters intracellular survival of *M.leprae*. Int J Lepr 72:16-26, 2004.
6) Kohsaka K, Mori T, Ito T: Lepromatoid lesion developed in nude mouse inoculated with *Mycobacterium leprae*. Lepro 45:177-187, 1976.
7) Nakamura M: Elimination of contaminants in a homogenate of nude-mouse footpad experimentally infected with *Mycobacterium leprae*. Jpn J Lepr 64:47-50, 1994.
8) Shepard CC, McRae DH: A method for counting acid-fast bacteria. Int J Lepr 36:78-82, 1968.
9) Adams LB, Franzblau S, Taintor R, Hibbs J Jr, Krahenbuhl JL: L- arginine-dependent macrophage effector functions inhibit metabolic activity of *Mycobacterium leprae*. J Immunol 147: 1642- 1646, 1991.
10) Maeda Y, Mukai T, Spencer J, Makino M: Identification of an immunomodulating agent from *Mycobacterium leprae*. Infect Immun 73:2744-2750, 2005.
11) Franzblau SG: Oxidation of palmitic acid by *Mycobacterium leprae* in an axenic medium. J Clin Microbiol 2618-2624, 1988.
12) Truman RW, Krahenbuhl JL: Viable *Mycobacterium leprae* as a research reagent. Int J Lepr 69: 1-12, 2001.
13) Kirchheimer W F, Storrs EH: Attempts to establish the armadillo (*Dasypus novemcinctus*) as a model for the study of leprosy. Int J Lepr 39:693-702, 1971.
14) Fieldsteel AH, McIntosh AH: Attempts to cultivate and determine the maximum period of viability of *M.leprae* in tissue culture. Int J Lepr 40: 271-277, 1972.
15) Tsunawaki S, Sporn M, Ding A, Nathan C: Deactivation of macrophage by transforming growth factor-beta. Nature 334:260-262, 1988.
16) Ding A, Nathan CF, Graycar J, Derynck R, Stuehr DJ, Srimal S: Macrophage deactivating factor and transforming growth factors-beta 1, - beta 2 and -beta 3 inhibit induction of macrophage nitrogen oxide synthesis by IFN-gamma. J Immunol 145:940-944, 1990.
17) Hirsch CS, Yoneda T, Averill L, Ellner JJ, Toosi Z: Enhancement of tintracellular growth of *Mycobacterium tuberculosis* in human monocytes by transforming growth factor-1. J Inf Dis 170:1229-1237, 1994.
18) Fiorentino DF, Zlotnik A, Viera P, Mosmann TR, Howard M, Moore KW, O'Garra A: IL-10 acts on the antigen presenting cell to inhibit cytokine production by Th1 cells. J Immunol 146:3444-3451, 1991.
19) O'Garra A, Chang R, Go N, Hastings R, Haughton G, Howard M: Ly-1 B (B-1) cells are the main source of B cell - derived IL-10. Eur J Immunol 22:711-717, 1992.
20) Redpath S, Ghazal P, Gascoigne NR: Hijacking and exploitation of IL-10 by intracellular pathogens. Trends Microbiol 9:86-92, 2001.
21) Dugas N, Palacios-Calender M, Dugas B, Riveros-Moreno V, Delfraissy J, Kolb J, Moncada S: Regulation by endogenous IL-10 of the expression of nitric oxide synthase induced by ligation of CD23 in human macrophage. Cytokine 10:680-689, 1998.
22) Huang C, Stevens B, Nielsen E, Slovin P, Fang X, Nelson D, Skimming J: Interleukin-10 inhibition of nitric oxide biosynthesis involves suppression of CAT-2 transcription. Nitric Oxide 6:79-84, 2002.
23) Makino M, Maeda Y, Fukutomi Y, Mukai T: Contribution of GM-CSF on the enhancement of the T cell-stimulating activity of macrophages. Microbes Infect 91:70-77, 2007.

マクロファージ内におけるらい菌生存の温度依存性

福富康夫*[1)]、前田百美[1)]、松岡正典[2)]、牧野正彦[1)]

国立感染症研究所ハンセン病研究センター

1）病原微生物部

2）生体防御部

〔受付：2008年8月4日、掲載決定：2008年10月15日〕

キーワード：生存、ヒト、マウス、マクロファージ、らい菌

ハンセン病は細胞内寄生菌であるらい菌によって引き起こされる感染症である。らい菌は主にマクロファージとシュワン細胞に感染する。しかしながら、マウスやヒトマクロファージ内における生存・発育機構について詳細は明らかになっていない。本研究では放射性同位元素を用いた方法によりらい菌の生存率を評価した。そして、らい菌感染マクロファージを35度で培養する方が37度で培養するよりもらい菌の生存率を高い状態に保つことができることが判明した。また、免疫抑制性サイトカインであるIL-10を添加することにより3週間程度生存が維持されることが分かった。一方、IL-10未添加の場合、生存率は徐々に低下した。ヒトマクロファージの場合は、IL-10未添加の場合でも少なくとも4週間生存は維持された。しかしながら、37度で培養すると2週間以内に生存率は著明に低下した。これらの結果から、らい菌の細胞内における生存には温度が決定的な要因のひとつであることが判明した。

* Corresponding author:
国立感染症研究所ハンセン病研究センター病原微生物部第二室
〒189-0002　東村山市青葉町4-2-1
TEL：042-391-8211　FAX：042-394-9092
E-mail：fukutomi@nih.go.jp

A Signaling Polypeptide Derived from an Innate Immune Adaptor Molecule Can Be Harnessed as a New Class of Vaccine Adjuvant[1]

Kouji Kobiyama,[3]* Fumihiko Takeshita,[2,3]* Ken J. Ishii,[†§] Shohei Koyama,[‡§] Taiki Aoshi,[†] Shizuo Akira,[‡§] Asako Sakaue-Sawano,[¶] Atsushi Miyawaki,[¶] Yuko Yamanaka,[‖] Hisashi Hirano,[‖] Koichi Suzuki,[#] and Kenji Okuda*

Modulation of intracellular signaling using cell-permeable polypeptides is a promising technology for future clinical applications. To develop a novel approach to activate innate immune signaling by synthetic polypeptides, we characterized several different polypeptides derived from the caspase recruitment domain (CARD) of IFN-β promoter stimulator 1, each of which localizes to a different subcellular compartment. Of particular interest was, N′-CARD, which consisted of the nuclear localization signal of histone H2B and the IFN-β promoter stimulator 1CARD and which localized to the nucleus. This polypeptide led to a strong production of type I IFNs and molecular and genetic analyses showed that nuclear DNA helicase II is critically involved in this response. N′-CARD polypeptide fused to a protein transduction domain (N′-CARD-PTD) readily transmigrated from the outside to the inside of the cell and triggered innate immune signaling. Administration of N′-CARD-PTD polypeptide elicited production of type I IFNs, maturation of bone marrow-derived dendritic cells, and promotion of vaccine immunogenicity by enhancing Ag-specific Th1-type immune responses, thereby protecting mice from lethal influenza infection and from outgrowth of transplanted tumors in vivo. Thus, our results indicate that the N′-CARD-PTD polypeptide belongs to a new class of vaccine adjuvant that directly triggers intracellular signal transduction by a distinct mechanism from those engaged by conventional vaccine adjuvants, such as TLR ligands. *The Journal of Immunology,* **2009, 182: 1593–1601.**

Accumulating evidence from basic research and from clinical studies clearly indicates that type I IFNs are key to the elimination of viral infection (1, 2), suppression of tumor progression (3, 4), and to vaccine immunogenicity (5). Type I IFNs, such as IFN-α and -β, are produced from a wide variety of cell types upon viral infection or in response to foreign nucleic acids, such as DNA and RNA (6–8). Recent research has dissected and elucidated the molecular basis of the ability of the immune system to sense a variety of nucleic acids as pathogen-associated molecular patterns (9) or to sense the presence of aberrant self-DNA under dangerous situations (10, 11). RIG-I-like helicases (RLHs)[4] mediate innate immune signaling in human cells induced by immunostimulatory RNAs, such as 5′-triphosphate RNA or dsRNA, or right-handed B-form DNA (B-DNA) (12–14). RLHs trigger cellular signaling through adaptor molecules, such as IFN-β promoter stimulator 1 (IPS-1, also known as MAVS/VISA/Cardif), TNFR-associating factor (TRAF) 3, and TRAF family member-associated NF-κB activator (TANK), thereby coordinating the activation of IκB kinase (IKK) family members, such as NF-κB essential modulator, IKK-α, IKK-β, TANK-binding kinase 1 (TBK1), and inducible IKK (IKKi). Once activated by such cytoplasmic kinases, NF-κB, IFN regulatory factor 3 (IRF3), and IRF7 transmigrate into the nucleus and act as master regulators of type I IFN-related gene promoters (15).

These signaling molecules contain distinct domains, and thereby associate with specific target molecules and modulate downstream signal transmission. IPS-1 plays a central role in this signaling pathway and its caspase recruitment domain (CARD) forms the death domain fold, which is structurally similar to domains of Fas-associated via death domain and caspase family members (16). The CARD of IPS-1 is essential for signal transmission through homotypic interactions with the CARDs of upstream RLHs (9). Mitochondrial sorting of IPS-1 is also crucial for its canonical

*Department of Molecular Biodefense Research, Yokohama City University Graduate School of Medicine, Yokohama, Japan; †Department of Molecular Protozoology and ‡Host Defense, Research Institute for Microbial Diseases, Osaka University, Suita, Japan; §World Premier International Immunology Frontier Research Center, Osaka University, Suita, Japan; ¶Laboratory for Cell Function Dynamics, Advanced Technology Development Group, Brain Science Institute, RIKEN, Wako, Japan; ‖Kihara Institute for Biological Research, Yokohama City University Graduate School of Integrated Science, Totsuka, Japan; and #Department of Bioregulation, National Institute of Infectious Diseases, Higashimurayama-shi, Japan

Received for publication July 24, 2008. Accepted for publication November 19, 2008.

The costs of publication of this article were defrayed in part by the payment of page charges. This article must therefore be hereby marked *advertisement* in accordance with 18 U.S.C. Section 1734 solely to indicate this fact.

[1] This work was supported, in part, by the Strategic Research Project of Yokohama City University (K18022 to F.T.), the Advancement of Medical Sciences from Yokohama Medical Foundation (to F.T. and K.K.), the National Institute of Biomedical Innovation (to K.O.), the Yasuda Medical Foundation (to F.T.), the Uehara Memorial Foundation (to F.T.), and a Grant-in-aid for Scientific Research (20590477 to F.T.) from the Ministry of Education, Culture, Sports, Science, and Technology of Japan.

[2] Address correspondence and reprint requests to Dr. Fumihiko Takeshita, Department of Molecular Biodefense Research, Yokohama City University Graduate School of Medicine, 3-9 Fukuura, Kanazawaku, Yokohama, Japan. E-mail address: takesita@yokohama-cu.ac.jp

[3] K.K. and F.T. contributed equally to this work.

[4] Abbreviations used in this paper: RLH, RIG-I-like helicase; B-DNA, B-form DNA; IPS-1, IFN-β promoter stimulator 1; TRAF, TNFR-associating factor; TANK, TRAF family member-associated NF-κB activator; TBK1, TANK binding kinase 1; IKK, IκB kinase; IKKi, inducible IKK; IRF3, IFN regulatory factor 3; CARD, caspase recruitment domain; N′-CARD, fusion of the NH_2-terminal nuclear localization signal of histone H2B to the IPS-1 CARD; PTD, protein transduction domain; TMD, transmembrane domain; NLS, nuclear localization signal; NDH, nuclear DNA helicase II; ODN, oligodeoxynucleotide; flu vax, influenza split-product vaccine; DC, dendritic cell; FL, full length; BM-DC, bone marrow-derived dendritic cell.

signaling because human hepatitis C virus NS3/4A protease inactivates IPS-1 by cleaving a region adjacent to the transmembrane domain (TMD), which is required for IPS-1 localization to the mitochondrial outer membrane (17).

To develop a novel approach to modulate innate immune signaling by synthetic polypeptides, we generated several different IPS-1 CARD-fusion polypeptides, each of which localizes to a different subcellular compartment. Of interest, the nuclear localization of a fusion polypeptide between the nuclear localization signal (NLS) of histone H2B and the IPS-1 CARD (hereafter referred to as N′-CARD) activated a distinct signaling pathway initiated from the nucleus and led to a strong production of type I IFN. Molecular and genetic analyses showed that nuclear DNA helicase II (NDH) is critically involved in this signaling pathway. Fusion of N′-CARD to the protein transduction domain (PTD), originally derived from the HIV Tat protein (18), facilitated transduction of N′-CARD from outside to inside the cell without loss of its original intracellular function. Finally, we demonstrate that the N′-CARD-PTD polypeptide acts as a novel vaccine adjuvant by directly triggering innate intracellular immune signaling to augment vaccine immunogenicity. Such a mechanism is distinct from TLR-mediated signaling, which is engaged in innate immune activation by conventional vaccine adjuvants, such as monophosphoryl-lipid A (an LPS derivative) and CpG oligodeoxynucleotide (ODN).

Materials and Methods

Cells and reagents

HEK293, HeLa, RAW264.7, and TC-1 cells were purchased from American Type Culture Collection and maintained in DMEM supplemented with 10% FCS and 50 μg/ml penicillin/streptomycin. Sf9 cells were maintained in Sf900 II SFM (Invitrogen). LPS was purchased from Sigma-Aldrich. CpG ODN, 5′-ATC GAC TCT CGA GCG TTC TC-3′, was synthesized by Gene Design. Mouse GM-CSF and Flt3L were purchased from PeproTech. Influenza split-product vaccine (flu vax) was prepared at The Research Foundation for Microbial Diseases of Osaka University (Kanon-ji city, Kagawa, Japan) from the purified influenza virus A/New Caledonia/20/99 strain (H1N1) by sequential treatment with ether and formalin, according to the method of Davenport et al. (19, 20).

Expression plasmids

The IPS-1 expression plasmid was described previously (21). The IPS-1 CARD, aa 1–100 of the IPS-1 ORF, was PCR-amplified. Fusion cDNAs were generated by ligating aa 1–100 and 514–540 of IPS-1 ORF (CARD-TMD), aa 1–37 of histone H2B ORF and aa 1–100 of IPS-1 ORF (N′-CARD), N′-CARD and aa 514–540 of hIPS-1 ORF (N′-CARD-TMD), and were amplified by PCR. These fragments were introduced in-frame into pFLAG CMV5b (Sigma-Aldrich) or pGEX6P-2 (GE Healthcare). GST-N′-CARD was further fused to the PTD (Tyr-Ala-Arg-Ala-Ala-Ala-Arg-Gln-Ala-Arg-Ala) and introduced into pFastBac HT-B (Invitrogen). TBK1, IKKi, NDH, and chloride channel 1A (CC1A) cDNAs were amplified by PCR using a human spleen cDNA library (Takara). These fragments were introduced in-frame into pFLAG-CMV4 (Sigma-Aldrich), pCIneo-HA, pCAGGS-Flag-m1SECFP, pCAG-His Venus, or pcDNA3-RFP. The N′-CARD T54A expression plasmid was generated by site-directed mutagenesis, as described previously (22). The sequences of the PCR products were confirmed using an ABI PRISM Genetic Analyzer (PE Applied Biosystems).

Luciferase assay

The luciferase assay was conducted as described previously (23).

Confocal microscopy

HeLa cells were transfected with CARD-YFP, CARD-TMD-YFP, N′-CARD-YFP, N′-CARD-TMD-YFP, IPS-1-YFP, YFP-IKKi, YFP-TBK1, and/or mRFP-NDH and incubated for 48 h. In some cases, the cells were treated with Hoechst 33258 (Invitrogen) and/or MitoTracker reagent (Invitrogen) at 37°C for 15 min. Alternatively, HeLa cells were treated with CARD or N′-CARD-PTD for 30 min. Cells were treated with Hoechst 33258 for 15 min before fixation and incubation with mouse anti-FLAG M2-Cy3. After washing with PBS containing 1% BSA, the cells were examined under an FV 500 confocal microscope (Olympus).

Immunoprecipitation and immunoblotting

Immunoprecipitation and immunoblotting was performed as described previously (24) using anti-FLAG M2 (Sigma-Aldrich), anti-FLAG M2-HRP (Sigma-Aldrich), anti-HA (Covance), anti-HA-HRP (Roche Diagnostics), anti-ubiquitin-HRP (Santa Cruz Biotechnology), anti-NDH (provided by J. D. Parvin, Brigham and Women's Hospital, Boston, MA), anti-p-JNK, anti-p-p38, anti-p-ERK, and anti-β-actin (Cell Signaling Technology).

RNA interference

An siRNA targeting NDH mRNA (stealth RNAi) was chemically synthesized by Invitrogen (Carlsbad, CA): sense, 5′-AUU GCU UGC AAA UCA UGA UCC UGU U-3′; antisense, 5′-AAC AGG AUC AUG AUU UGC AAG CAA U-3′. HEK293 cells (6×10^5) were transfected with 120 pmol of control or NDH siRNA using Lipofectamine RNAi MAX reagent (Invitrogen) according to the manufacturer's protocol.

Purification of recombinant polypeptides

DH10Bac competent cells (Invitrogen) were transformed with pFastBac HT-B-GST or with GST-N′-CARD-PTD to generate recombinant Bacmids. Sf9 cells were transfected with Bacmid-encoding GST or GST-N′-CARD-PTD to generate recombinant seed baculoviruses. Seventy-two hours after infection, the Sf9 cells were washed once with PBS and suspended in sonication buffer (50 mM Tris-HCl (pH 8.0), 50 mM NaCl, 1 mM EDTA, 1 mM DTT) containing 10% Triton X-100. After sonication, cell lysates were centrifuged at 15,000 rpm, at 4°C for 30 min. The supernatants were collected and dialyzed with sonication buffer. Recombinant polypeptides were purified using GSTrap (GE Healthcare) according to the manufacturer's protocol. In brief, after the column was equilibrated with 2 ml sonication buffer, the cell lysate was applied and the column then washed three times with 10 ml PBST (PBS containing 0.5% Triton X-100) and with PBS once. Recombinant polypeptide (GST or GST-N′-CARD-PTD) was eluted with sonication buffer containing 10 mM reduced glutathione and then dialyzed with PBS. Recombinant proteins (1 μg) used in all the experiments contained <20 fg endotoxins (*Limulus* J Single Test, Wako).

ELISA and RT-PCR

Bone marrow-derived dendritic cells (DCs) were generated by 5 days of culture with GM-CSF (20 ng/ml) (GM-DCs) or Flt3L (100 ng/ml) (FL-DCs). GM-DCs or FL-DCs were treated with or without 1, 3, or 10 μg/ml N′-CARD-PTD or 1 μM of CpG ODN for 24 h and the supernatants were subjected to ELISA for mouse IFN-α, IFN-β (PBL Biomedical Laboratories), or IL-12 p40 (Invitrogen). RAW264.7 cells were treated with 1 μg/ml LPS or 10 μg/ml N′-CARD-PTD for 3, 6, 12, 18, 24, and 48 h. The levels of mRNA for TNF-α, IL-6, IFN-α, IFN-β, IP-10, and β-actin were examined by RT-PCR as described previously (5, 22).

Immunization

Eight-week-old female BALB/c mice were administered s.c. with N′-CARD-PTD (5 μg), CpG ODN (5 μg), or flu vax (0.7 μg) alone, flu vax (0.7 μg) plus N′-CARD-PTD (5 μg), or flu vax (0.7 μg) plus CpG ODN (5 μg) at 0 and 10 days. Blood was drawn at 20 days and serum Ab titer was measured by ELISA as described previously (25). Alternatively, 8-wk-old female C57BL/6 mice were immunized with E7 peptide (E7, Arg-Ala-His-Tyr-Asn-Ile-Val-Thr-Phe, 3 μg), E7 plus N′-CARD-PTD (5 μg), or E7 plus CpG ODN (5 μg) at 0 and 2 wk. Splenocytes were harvested 2 wk after final immunization. The cells were incubated with 1 μg/ml E7 or NP peptide (Ala-Ser-Asn-Glu-Asn-Met-Glu-Thr-Met) for 18 h at 37°C. Total RNA was isolated and real-time PCR was performed as described previously (22).

Influenza challenge

Ten days after final immunization, mice were challenged intranasally with 2×10^4 pfu (8 LD_{50}) of influenza virus A/PR/8/34 (25). The body weights and mortality of the challenged mice were monitored for the next 14 days.

Tumor transplantation

Eight week-old C57BL/6 mice were administered subcutaneously with TC-1 (1×10^5 cells/mouse), a mouse lung carcinoma expressing E7 Ag (25). Mice were immunized with control NP peptide (3 μg), E7 (3 μg), N′-CARD-PTD (5 μg), or E7 (3 μg) plus N′-CARD-PTD (5 μg) at 3, 4, 5, 6, and 7 day after TC-1 inoculation. The sizes of local tumor mass were monitored for the next 20 days.

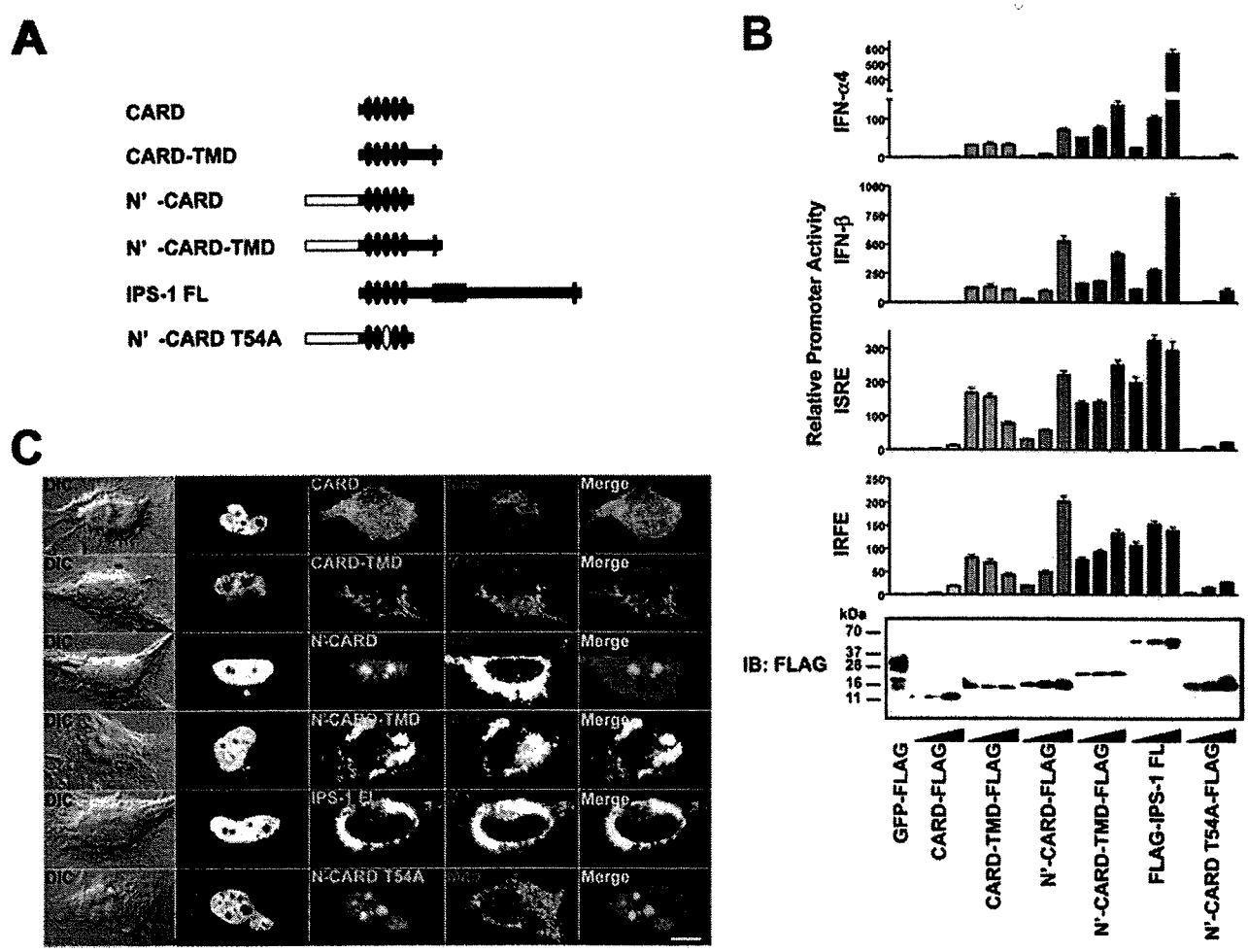

FIGURE 1. Synthetic IPS-1 CARD fusion molecules induce activation of type I IFN-related promoters. *A*, Schematic diagram of synthetic fusion molecules consisting of domains derived from IPS-1 and histone H2B. *B*, HEK293 cells were transfected with the expression plasmids, GFP-FLAG, CARD-FLAG, CARD-TMD-FLAG, N′-CARD-FLAG, N′-CARD-TMD-FLAG, FLAG-IPS-1 FL, and N′-CARD T54A-FLAG in the presence of TK-RL plus a reporter plasmid expressing firefly luciferase under the control of either the IFN-α4 promoter (*top panel*), the IFN-β promoter (*second panel from the top*), the ISRE-dependent promoter (*third panel from the top*), or the IRFE-dependent promoter (*fourth panel from the top*). Data represent means ± SD of the relative luciferase activity of six samples. Cell lysates were also subjected to immunoblot analysis to examine levels of target polypeptide expression (*bottom panel*). *C*, HeLa cells were transfected with the expression plasmids, YFP-CARD, YFP-CARD-TMD, YFP-N′-CARD, YFP-N′-CARD-TMD, YFP-IPS-1 FL, and YFP-N′-CARD T54A. Genomic DNA or mitochondria were stained with Hoechst 33258 or Mitotracker reagent, respectively, and then analyzed under a confocal microscope. The data represent one of three independent experiments with similar results. Scale bar, 10 μm.

Statistical analysis

The Student's *t* test or the Mantel-Cox log rank test was used for statistical analysis.

Results

The nuclear redistribution of IPS-1 CARD elicits type I IFN promoter activation

To elucidate the mechanisms underlying IPS-1 CARD-mediated signaling, plasmids encoding either the IPS-1 CARD alone or the IPS CARD fused to the IPS-1 TMD or to the NLS of histone H2B were generated and their abilities to induce type I IFN-related promoter activation were characterized (Fig. 1*A*). Although the CARD alone had minimal activity in eliciting such promoter activation, fusion of the TMD to the CARD (CARD-TMD) resulted in a significant activation, suggesting that the TMD facilitates CARD-mediated signaling, consistent with previous data (Fig. 1*B*; Ref. 26). Of interest, fusion of the NH_2-terminal NLS of histone H2B to the IPS-1 CARD (N′-CARD) conferred strong promoter activation, suggesting that nuclear localization of N′-CARD triggers signal activation. Indeed, N′-CARD induced phosphorylation of IRF3 at a comparable level to full length IPS-1 (FL) (Supplemental Fig. 1).[5] The mutant polypeptide N′-CARD T54A, in which the third α-helical structure of the CARD was disrupted (22), induced significantly lower levels of promoter activation, suggesting that the conformation of the IPS-1 CARD is also critical for its activity. Although N′-CARD fused to the IPS-1 TMD (N′-CARD-TMD) induced significant levels of promoter activation, the levels were comparable to those induced by N′-CARD or CARD-TMD, suggesting that the effects of CARD distribution mediated by the NLS and the IPS-1 TMD are redundant.

N′-CARD localizes to the nucleus and signals through NDH

To elucidate the signaling mechanisms triggered by N′-CARD and CARD-TMD, we examined the subcellular localizations of these fusion molecules. Confocal microscopy analysis showed that CARD-TMD fused to YFP (YFP-CARD-TMD) was present in

[5] The online version of this article contains supplemental information.

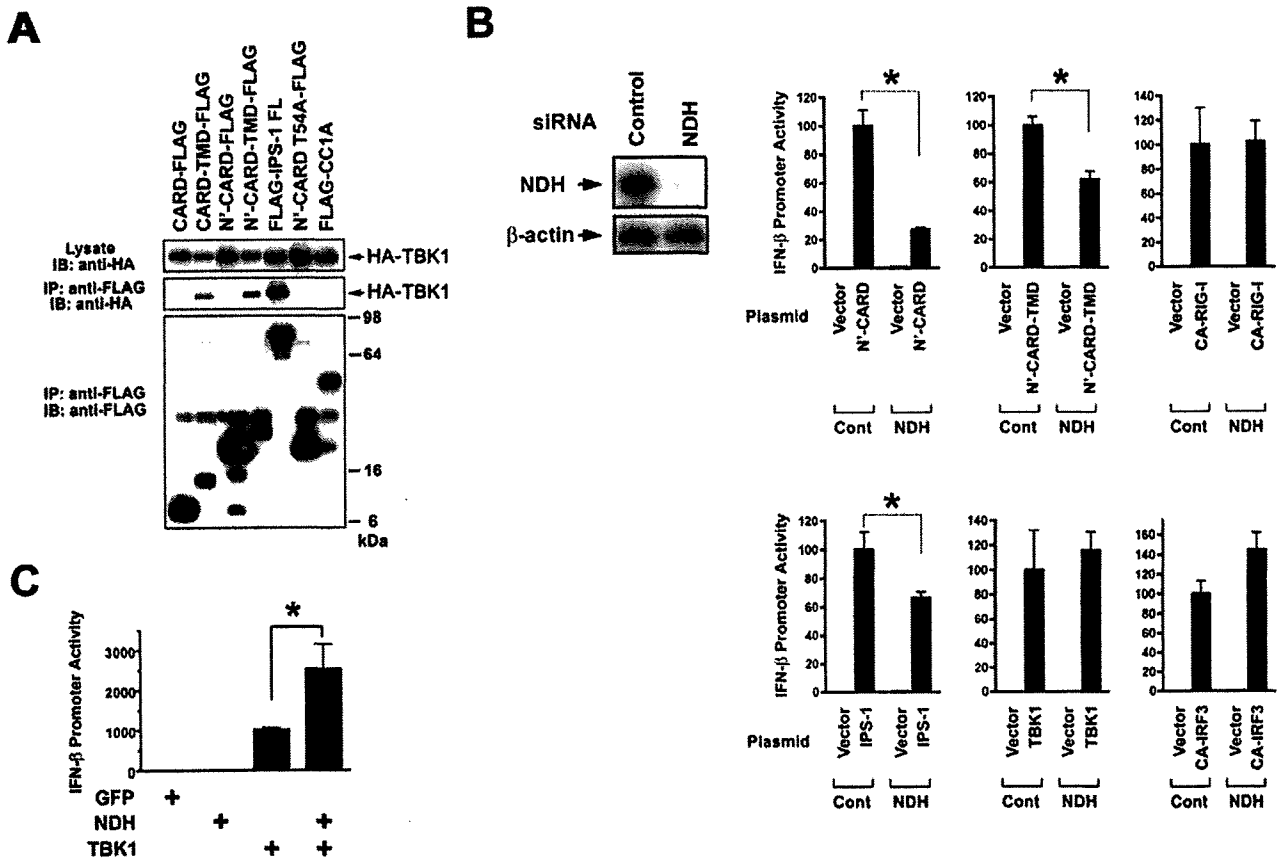

FIGURE 2. Role of NDH in N′-CARD-mediated signaling. *A*, Cell lysates from HEK293 cells transfected with the expression plasmids for HA-TBK1 plus CARD-FLAG, CARD-TMD-FLAG, N′-CARD-FLAG, N′-CARD-TMD-FLAG, FLAG-IPS-1 FL, N′-CARD T54A-FLAG, or FLAG-CC1A were prepared and immunoprecipitated with anti-FLAG Ab. The immune complexes were analyzed by immunoblotting using anti-HA or anti-FLAG Ab. *B*, After HEK293 cells were transfected with control or NDH siRNA, the levels of NDH protein were examined by immunoblotting. The cells were further transfected with the expression plasmid for N′-CARD, N′-CARD-TMD, CA-RIG-I, IPS-1, TBK1, and CA-IRF3 in the presence of TK-RL plus a reporter plasmid expressing firefly luciferase under the control of the IFN-β promoter. *C*, HEK293 cells were transfected with the expression plasmid(s) for GFP, NDH, and/or TBK1 in the presence of TK-RL plus a reporter plasmid expressing firefly luciferase under the control of the IFN-β promoter. *B* and *C*, Forty eight hours after transfection, luciferase assay was performed. Data represent means ± SD of the relative luciferase activity of eight samples. *, $p < 0.05$.

mitochondria, with a localization pattern similar to that of IPS-1 FL (YFP-IPS-1 FL), while N′-CARD fused to YFP (YFP-N′-CARD) was mostly present in the nuclear interchromosomal space (Fig. 1*C*). Because CARD alone (YFP-CARD) was present diffusely within the cell and both YFP-N′-CARD and YFP-N′-CARD T54A localized to the nucleus, it was suggested that the NLS directed the nuclear distribution of the IPS-1 CARD (Fig. 1*C*). These results implied that N′-CARD triggers cellular signaling pathways that originate in the nucleus and that are distinct from those triggered by CARD-TMD or IPS-1 FL, which originate from mitochondria.

TBK1, and its closely related IKK family member IKKi, are kinases acting downstream of IPS-1 and are required for a type I IFN production (21, 26, 27). We next examined the molecular interactions between each CARD-fusion molecule and TBK1 by immunoprecipitation analysis. As a control, TBK1 was coprecipitated with IPS-1 FL (Fig. 2*A*). A significant amount of TBK1 was also detected after precipitation with CARD-TMD or N′-CARD-TMD, but not after precipitation with CARD, N′-CARD, or N′-CARD T54A, suggesting that the TMD supports the association of the CARD with TBK1 (Fig. 2*A*).

To examine the signaling mechanisms triggered by N′-CARD, we tried to identify cellular molecules that associate with N′-CARD using a tandem-affinity purification system and TOF-MS analysis (data not shown). Among the N′-CARD interacting molecules identified, we were particularly interested in nuclear DNA helicase II (NDH, also known as RNA helicase A), a 1270 amino acid protein containing two copies of a dsRNA binding domain, a DEIH (Asp-Glu-Ile-His) helicase core, and an RGG (Arg-Gly-Gly) box nucleic acid-binding domain.

To examine the functional role of NDH in the signaling pathway leading to type I IFN production, NDH mRNA was ablated by RNA interference. Endogenous NDH protein was specifically decreased by NDH siRNA but not by control siRNA treatment (Fig. 2*B*). Knockdown of NDH resulted in a suppression of N′-CARD-induced IFN-β promoter activation by 73%. The level of promoter activation induced by IPS-1 or N′-CARD-TMD was also partially suppressed in NDH-knockdown cells by 33 and 38%, respectively. The levels were comparable when a constitutively active form of RIG-I (RIG-I 2CARDs), TBK1, or a constitutively active form of IRF3 (IRF3CA) was examined (Fig. 2*B*). Although over-expression of NDH had no effect, and over-expression of TBK-1 had a minimal effect on IFN-β promoter activation, over-expression of NDH plus TBK1 synergistically activated the IFN-β promoter, suggesting that NDH had the ability to up-regulate TBK1 activity (Fig. 2*C*). These results, taken together, suggest that NDH is involved in the events downstream of N′-CARD, and partially in

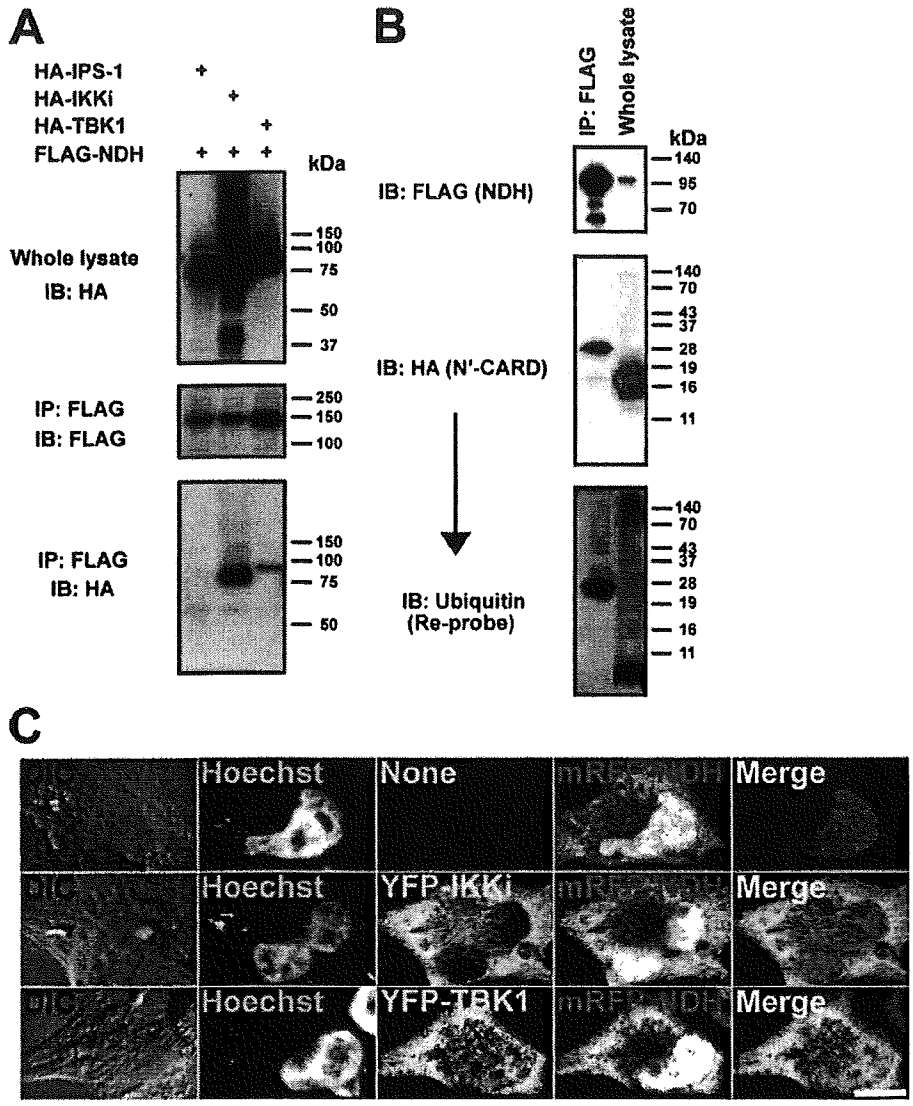

FIGURE 3. NDH associates with N′-CARD, TBK1, and IKKi. *A* and *B*, The lysates of HEK293 cells transfected with the expression plasmids for FLAG-NDH plus HA-IPS-1, HA-IKKi, HA-TBK1 (*A*) or N′-CARD-HA (*B*) were prepared and immunoprecipitated with anti-FLAG Ab. The immunoblots were probed with anti-HA or anti-FLAG Ab (*A* and *B*) or sequentially probed with anti-HA and anti-ubiquitin Ab (*B*). *C*, HeLa cells were transfected with an expression plasmid for mRFP-NDH alone or with those for mRFP-NDH and YFP-IKKi or YFP-TBK1. After staining with Hoechst 33258, the cells were examined under a confocal microscope. Data represent one of three independent experiments with similar results. Scale bar, 10 μm.

those downstream of IPS-1, and that it plays a role in signaling upstream of TBK1.

To confirm the physical interactions among NDH, IKKi, TBK1, and N′-CARD, immunoprecipitation analysis was performed. A strong interaction was detected between NDH and IKKi or TBK1, while there was no apparent association of NDH with IPS-1 in this assay (Fig. 3*A*). By contrast, NDH was confirmed to interact with N′-CARD. Of interest, the mobility of N′-CARD coprecipitated with NDH was retarded in SDS-PAGE (~25 kDa) when compared with that in whole cell lysate (~18 kDa) (Fig. 3*B*). The retarded N′-CARD was detected by anti-ubiquitin Ab, suggesting that mono-ubiquitinated N′-CARD, directly or indirectly, has the ability to associate with NDH (Fig. 3*B*). We also examined the subcellular localization of NDH, IKKi, and TBK1 by confocal microscopy analysis (Fig. 3*C*). Both YFP-IKKi and YFP-TBK1 were mostly present in the cytoplasm, while mRFP-NDH was diffusely present within the cell. Most NDH present within the cytoplasm colocalized with IKKi or TBK1 (Fig. 3*C*).

Recombinant N′-CARD polypeptide fused to the protein transduction domain (N′-CARD-PTD) induces type I IFN production and exerts innate immune responses in vitro

To examine the potent ability of N′-CARD in modulating innate immune responses, we generated a recombinant N′-CARD polypeptide fused to the PTD, which enables transduction of extracellular protein into intracellular compartments. When the N′-CARD-PTD polypeptide was added to the culture medium of HeLa cells, it entered the nucleus within 30 min (Fig. 4*A*). By contrast, when the same amount of CARD polypeptide was added, only a minimal level of the polypeptide was observed inside the cell (Fig. 4*A*). The addition of the N′-CARD-PTD polypeptide alone induced significant levels of IFN-β promoter activation in HEK293 cells, suggesting that N′-CARD-PTD has the ability to transmigrate into the cell and trigger NDH-mediated cellular signaling to elicit type I IFN production (Supplemental Fig. 2).

We next examined whether administration of the N′-CARD-PTD polypeptide activates immune cells in vitro. As shown in Fig. 4*B*, N′-CARD-PTD induced production of a proinflammatory cytokine (TNF-α), type I IFNs (IFN-α and -β), and an IFN-stimulated gene product (IP-10) in a mouse macrophage cell line, RAW264.7. The expression of IFN-α and -β mRNAs was detected within 18 h; the expression of IFN-α mRNA continued for more than 48 h after N′-CARD-PTD treatment. By contrast, LPS, an activator of TLR4-mediated innate immune responses, induced IFN-β mRNA within 3 h, but this induction lasted for less than 18 h. The overall level of IFN-α mRNA production was higher in cells stimulated with N′-CARD-PTD compared with those stimulated with LPS, while that of IFN-β was lower in those stimulated

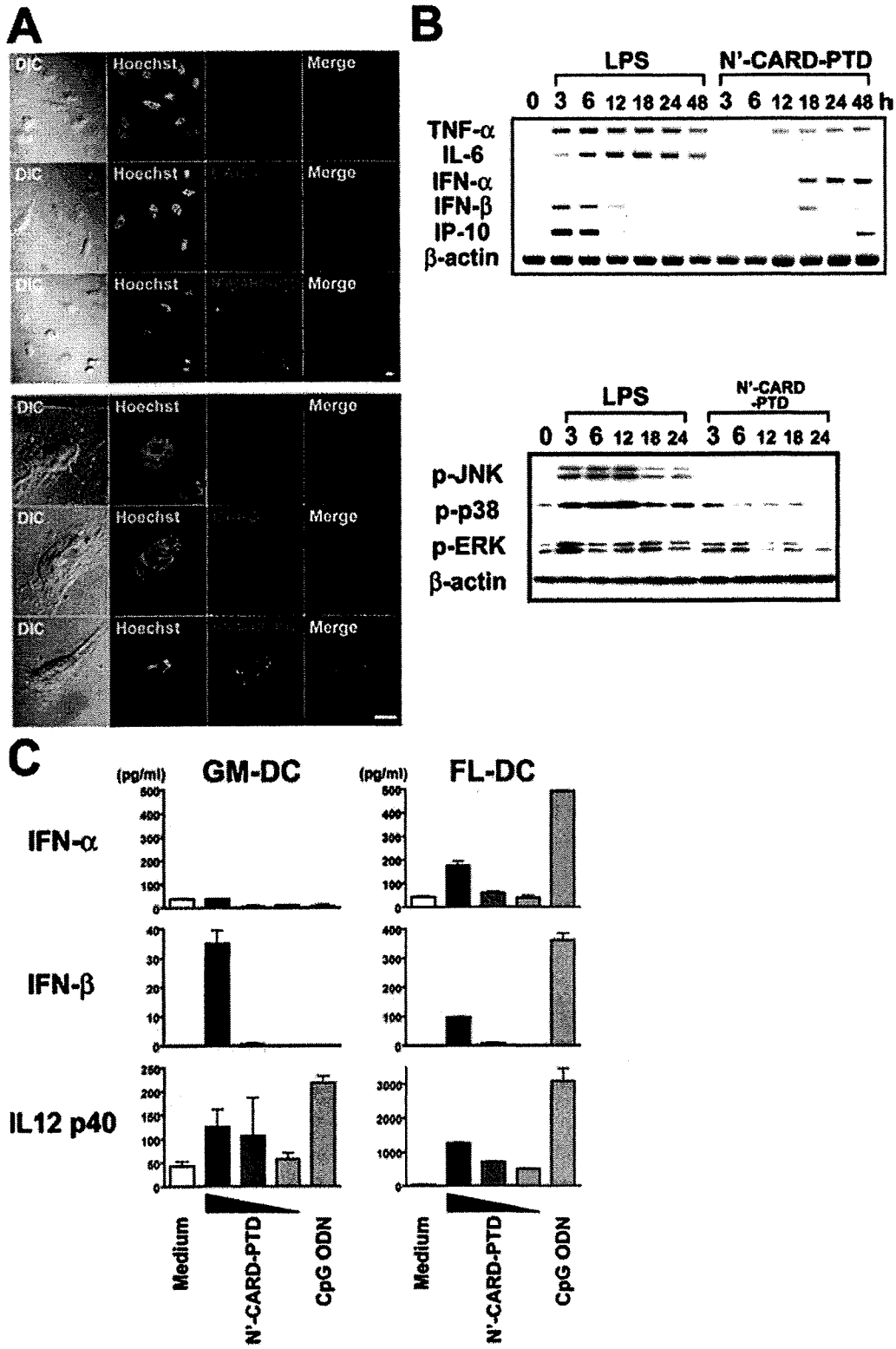

FIGURE 4. The N'-CARD-PTD polypeptide induces type I IFN production and DC maturation. *A*, Recombinant CARD or N'-CARD-PTD polypeptide was administered into the culture medium of HeLa cells. Thirty minutes after addition, the cells were permeabilized, stained with anti-FLAG M2-Cy3 and Hoechst 33258, and subjected to confocal microscopy analysis. *Upper panel*, Lower magnification. *Lower panel*, Higher magnification. Scale bar, 10 μm. *B*, RAW264.7 cells were treated with 1 μg/ml LPS or 10 μg/ml N'-CARD-PTD for 3, 6, 12, 18, 24, and 48 h. The levels of mRNA expression for TNF-α, IL-6, IFN-α, IFN-β, IP-10 and β-actin were examined by RT-PCR (*upper panel*). The levels of phosphorylated JNK, p38, or ERK were examined by immunoblotting (*lower panel*). *C*, GM-DCs or FL-DCs were treated with or without 1, 3, or 10 μg/ml N'-CARD-PTD or 1 μM of CpG ODN for 24 h and the supernatants were subjected to ELISA for mouse IFN-α, IFN-β, or IL-12 p40. Data represent one of two or three independent experiments with similar results.

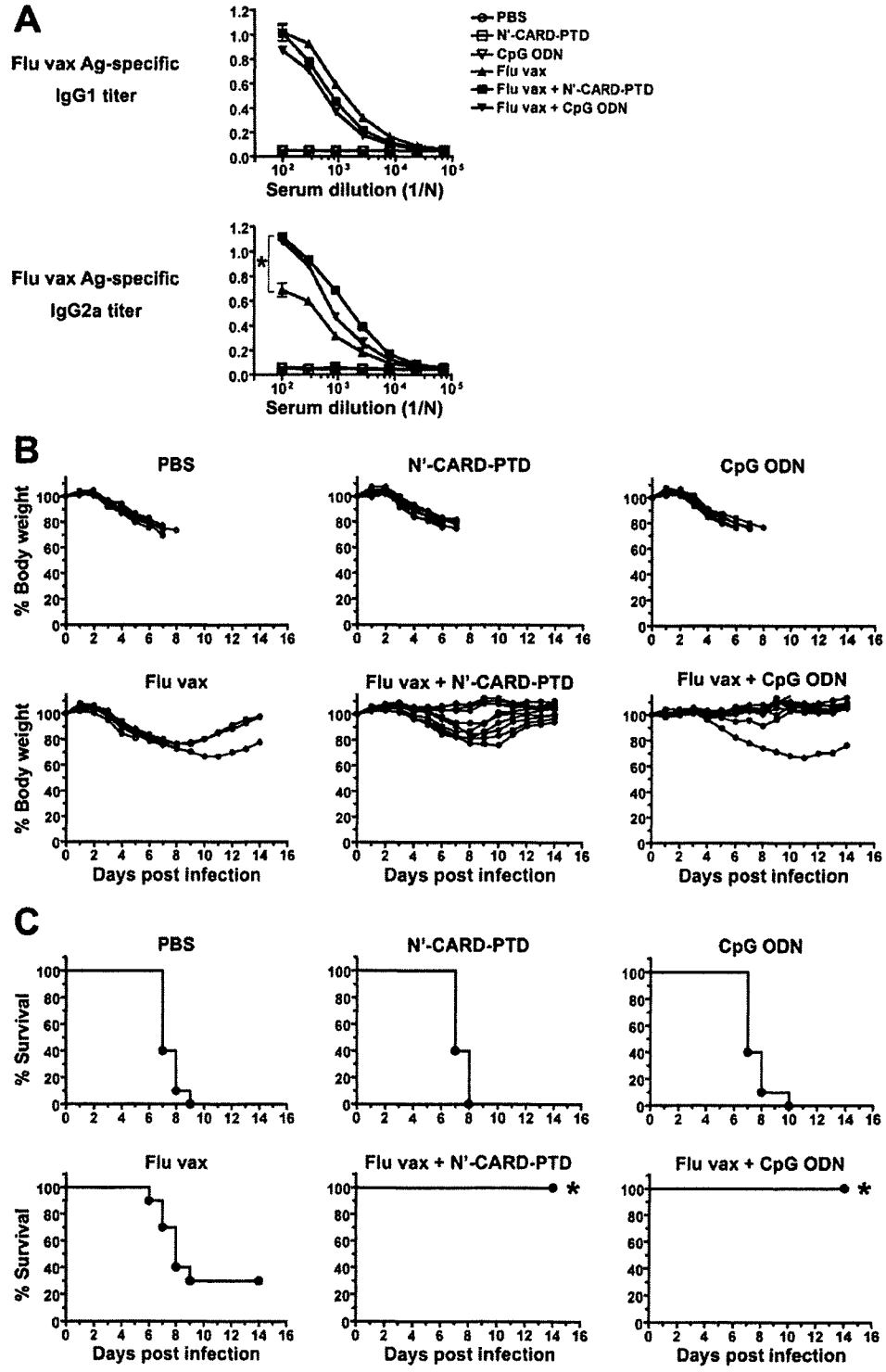

FIGURE 5. Coadministration of N′-CARD-PTD enhances Ag-specific IgG2a production and superior protection against lethal influenza infection. *A–C*, Eight-week-old female BALB/c mice (n = 10) were immunized s.c. with flu vax (0.7 μg), N′-CARD-PTD (5 μg), CpG ODN (5 μg), flu vax (0.7 μg) plus N′-CARD-PTD (5 μg), or flu vax (0.7 μg) plus CpG ODN (5 μg) at 0 and 10 days. *A*, Anti-flu vax Ab titer was examined 10 days after the final immunization. *B* and *C*, Ten days after the final immunization, mice were challenged with 8 LD_{50} doses of influenza A/P/R8 (H1N1). The body-weight changes (*B*) and the mortality (*C*) were monitored for the next 14 days. Data represent one of two independent experiments with similar results. *, $p < 0.05$.

with N′-CARD-PTD compared with those stimulated LPS (Fig. 4*B*). These results suggest that N′-CARD-PTD activates a distinct innate immune signaling pathway(s) from those engaged by LPS. In fact, LPS induced phosphorylation of MAPK such as JNK, p38, and ERK within 3 h, while N′-CARD-PTD had little effects on activation of these kinases except for ERK at 3 and 6 h (Fig. 4*B*). We also examined whether N′-CARD-PTD activates bone marrow-derived dendritic cells (BM-DCs). As a control, CpG ODN activated BM-DCs induced in vitro by Flt3L (FL-DCs) but not BM-DCs induced in vitro by GM-CSF (GM-DCs) to produce type I IFNs. N′-CARD-PTD, by contrast, activated both GM-DCs and FL-DCs to produce type I IFNs (Fig. 4*C*). We also observed that N′-CARD-PTD weakly but significantly up-regulated cell surface expression of MHC class I, class II, CD40, and CD86 on both GM-DCs and FL-DCs (data not shown). Up-regulation of such cell surface molecules was dependent on type I IFN production but independent on myeloid differentiation factor 88 (MyD88) nor Toll-IL-1R domain-containing adaptor-inducing IFN-β (TRIF) (data not shown).

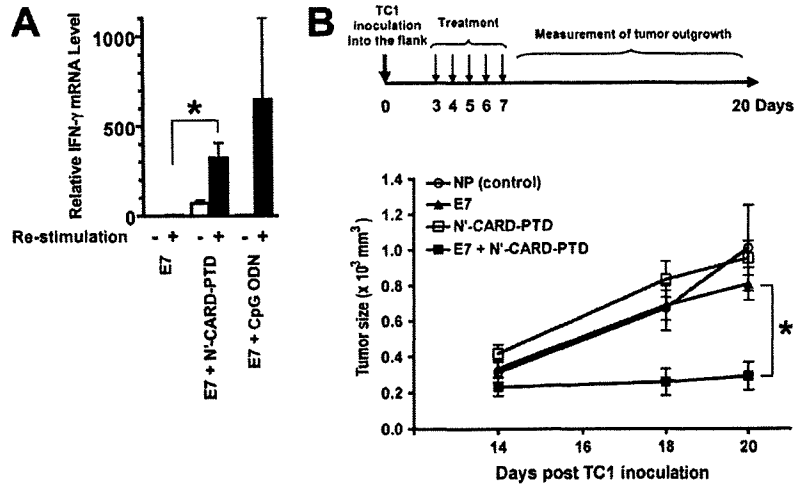

FIGURE 6. Coadministration of N'-CARD-PTD plus tumor-associated Ag E7 confers superior protection against tumor outgrowth. *A*, Eight-week-old female BALB/c mice ($n = 5$) were immunized subcutaneously with E7 peptide (3 μg), E7 peptide (3 μg) plus N'-CARD-PTD (5 μg), or E7 peptide (3 μg) plus CpG ODN (5 μg) at 2 and 4 wk. Splenocytes were prepared from each individual mouse and restimulated in vitro with control NP (−) or E7 peptide (±). The relative expression levels of IFN-γ mRNA were measured by real-time PCR and normalized to 18S rRNA levels. *B*, Eight-week-old C57BL/6 mice ($n = 10$) were inoculated subcutaneously with 1×10^5 TC-1 cells/mouse at 0 days and then immunized with control NP peptide (3 μg), E7 (3 μg), N'-CARD-PTD (5 μg), or E7 (3 μg) plus N'-CARD-PTD (5 μg) at 3, 4, 5, 6, and 7 days. Tumor sizes were measured at 14, 18, and 20 days. Data represent one of two independent experiments with similar results. *, $p < 0.01$.

N'-CARD-PTD augments Ag-specific acquired immune responses to protect against influenza virus infection and tumor outgrowth in vivo

To examine the in vivo effects of N'-CARD-PTD on innate and acquired immune responses, we used a mouse model of influenza virus infection and of tumor transplantation. Influenza split-product vaccine (flu vax) was used to evaluate the adjuvanticity of N'-CARD-PTD. Flu vax was prepared at The Research Foundation for Microbial Diseases of Osaka University from the purified influenza virus A/New Caledonia/20/99 strain treated sequentially with ether and formalin. As shown in Fig. 5*A*, s.c. administration of flu vax plus N'-CARD-PTD or CpG ODN induced significant levels of specific IgG1 production that were comparable to that of flu vax alone. Administration of flu vax plus N'-CARD-PTD or CpG ODN, by contrast, resulted in significantly higher levels of specific IgG2a production compared with that of flu vax alone, suggesting that N'-CARD-PTD and CpG ODN have the ability to modulate Th1-deviated immune responses. In accordance with such adjuvant effects, immunization with flu vax plus N'-CARD-PTD conferred superior protection against a lethal influenza challenge relative to that with flu vax alone (Fig. 5, *B* and *C*).

We next examined whether N'-CARD-PTD has an ability to enhance Ag-specific cellular immune responses. Immunization with MHC class I-restricted HPV E7 peptide (E7) alone induced minimal levels of E7-specific IFN-γ production from splenocytes (Fig. 6*A*). Treatment with E7 plus N'-CARD-PTD or CpG ODN induced higher levels of E7-specific IFN-γ production, suggesting that N'-CARD-PTD has an adjuvant effect on cell-mediated immune responses (Fig. 6*A*). Thus, mice were s.c. transplanted with TC-1 cells expressing E7 as a model tumor Ag, and then immunized with E7 in the presence or absence of N'-CARD-PTD, as shown in Fig. 6*B*. The outgrowth of TC-1 tumors in mice treated with either N'-CARD-PTD or E7 alone was comparable to that in mice treated with control NP peptide. In accordance with E7-specific IFN-γ production from splenocytes, the sizes of established tumors in mice treated with E7 plus N'-CARD-PTD were significantly smaller compared with those in mice treated with E7 alone or with N'-CARD-PTD alone (Fig. 6*B*). These in vivo results, taken together, indicate that N'-CARD-PTD, an activator of NDH-mediated innate immune responses, acts as a vaccine adjuvant, thereby enhancing protective immune responses against pathogens or tumors.

Discussion

This study provides the first evidence that the N'-CARD-PTD polypeptide directly enters the nucleus and triggers the innate immune signaling pathway leading to type I IFN production through NDH. NDH is a member of the DEXH (Asp-Glu-X-His) family of helicases and is highly conserved in higher eukaryotes, from *Drosophila* to mammals. Previous studies have shown that NDH interacts with molecules of the transcription machinery, such as the RNA polymerase II complex (28), cAMP-response element-binding protein (28), and NF-κB p65 (29), thereby regulating the transcription of responsive genes. NDH also acts together with the RNA editing enzyme to coordinate the editing and splicing of numerous cellular and viral RNAs (30, 31). Knockout of the *Ndh* gene led to early embryonic lethality (<E10.5) due to a high frequency of apoptosis in embryonic ectodermal cells during gastrulation (32). In addition to these properties of gene regulation and cellular homeostasis, our results suggest that NDH has a distinct property of mediating innate immune signaling upstream of TBK1. Recently, it was shown that a DEAD (Asp-Glu-Ala-Asp) box helicase, DDX3X, is a kinase substrate of TBK1 and acts as a critical component of TBK1-dependent innate immune signaling, particularly in the type I IFN production pathway (33).

MAPK activation plays a significant role in LPS- or CpG DNA-mediated signaling (Fig. 4*C* and Ref. 34), however, the signaling pathway induced by N'-CARD-PTD may not involve MAPK. This suggested that, unlike TLR-mediated signaling pathways, activation of MAPK is not crucial for N'-CARD-PTD-mediated type I IFN production. Rather, the action of N'-CARD-PTD resembles the signal activation induced by IFN stimulatory DNA, which was originally reported by Stetson et al. as having a similar action to B-DNA, which is critical in the control of DNA vaccine immunogenicity (5, 35). Because MAPK activation is associated with deleterious effects, ranging from hyperinflammation to cancer (36), the lack of such kinase activation would be an advantage for the repeated clinical application of N'-CARD-PTD. Further study will be needed to elucidate the molecular basis of the NDH-mediated signaling pathway and to determine the value of N'-CARD-PTD for clinical use.

Many TLR ligands and related compounds have been tested as vaccine adjuvants and as anti-allergy and anti-cancer drugs in humans (37). Among these, some clinical trials of TLR9-targeting molecules, including CpG ODN and its conjugated products, have recently been abandoned due to unexpectedly weaker responses in

humans relative to those observed in mice. This result was attributable to a lower frequency of TLR9 expression in human immune cells; expression was found in only a portion of B cells and plasmacytoid DCs that combined made up just 1% of the total immune cell population (38). In contrast, immunostimulatory RNA or B-DNA activates innate immune responses through cytosolic receptors but only when they are introduced into intracellular compartments, i.e., they have almost no effects when they are present outside the cell. Taking such observations into account, N′-CARD-PTD may have the advantage of self-transmigration into the nucleus and of triggering innate immune signaling in the absence of TLRs but in the presence of NDH and TBK1, which are ubiquitously expressed in a wide-variety of cell types.

In conclusion, this study showed concrete evidence that the activation of a distinct NDH-mediated signaling pathway up-regulates innate immune responses and that N′-CARD-PTD is a candidate vaccine adjuvant in future vaccine development. These findings may also provide insights that will be helpful in the design of immunomodulatory agents, such as using constitutively active signaling molecules of the innate immune responses.

Disclosures

The authors have no financial conflict of interest.

References

1. Barr, S. D., J. R. Smiley, and F. D. Bushman. 2008. The interferon response inhibits HIV particle production by induction of TRIM22. *PLoS Pathog.* 4: 1–11.
2. Fodil-Cornu, N., and S. M. Vidal. 2008. Type I interferon response to cytomegalovirus infection: the kick-start. *Cell Host Microbes* 3: 59–61.
3. Bracci, L., E. Proietti, and F. Belardelli. 2007. IFN-α and novel strategies of combination therapy for cancer. *Ann. NY Acad. Sci.* 1112: 256–268.
4. Ferrantini, M., I. Capone, and F. Belardelli. 2007. Interferon-α and cancer: mechanisms of action and new perspectives of clinical use. *Biochimie* 89: 884–893.
5. Ishii, K. J., T. Kawagoe, S. Koyama, K. Matsui, H. Kumar, T. Kawai, S. Uematsu, O. Takeuchi, F. Takeshita, C. Coban, and S. Akira. 2008. TANK-binding kinase-1 delineates innate and adaptive immune responses to DNA vaccines. *Nature* 451: 725–729.
6. Ishii, K. J., C. Coban, H. Kato, K. Takahashi, Y. Torii, F. Takeshita, H. Ludwig, G. Sutter, K. Suzuki, H. Hemmi, et al. 2006. A Toll-like receptor-independent antiviral response induced by double-stranded B-form DNA. *Nat. Immunol.* 7: 40–48.
7. Zhu, J., X. Huang, and Y. Yang. 2007. Innate immune response to adenoviral vectors is mediated by both Toll-like receptor-dependent and -independent pathways. *J. Virol.* 81: 3170–3180.
8. Takeuchi, O., and S. Akira. 2008. MDA5/RIG-I and virus recognition. *Curr. Opin. Immunol.* 20: 17–22.
9. Kawai, T., and S. Akira. 2007. Antiviral signaling through pattern recognition receptors. *J. Biochem.* 141: 137–145.
10. Yoshida, H., Y. Okabe, K. Kawane, H. Fukuyama, and S. Nagata. 2005. Lethal anemia caused by interferon-β produced in mouse embryos carrying undigested DNA. *Nat. Immunol.* 6: 49–56.
11. Kawane, K., M. Ohtani, K. Miwa, T. Kizawa, Y. Kanbara, Y. Yoshioka, H. Yoshikawa, and S. Nagata. 2006. Chronic polyarthritis caused by mammalian DNA that escapes from degradation in macrophages. *Nature* 443: 998–1002.
12. Kato, H., O. Takeuchi, S. Sato, M. Yoneyama, M. Yamamoto, K. Matsui, S. Uematsu, A. Jung, T. Kawai, K. J. Ishii, et al. 2006. Differential roles of MDA5 and RIG-I helicases in the recognition of RNA viruses. *Nature* 441: 101–105.
13. Cheng, G., J. Zhong, J. Chung, and F. V. Chisari. 2007. Double-stranded DNA and double-stranded RNA induce a common antiviral signaling pathway in human cells. *Proc. Natl. Acad. Sci. USA* 104: 9035–9040.
14. Takahasi, K., M. Yoneyama, T. Nishihori, R. Hirai, H. Kumeta, R. Narita, M. Gale, Jr., F. Inagaki, and T. Fujita. 2008. Nonself RNA-sensing mechanism of RIG-I helicase and activation of antiviral immune responses. *Mol. Cell* 29: 428–440.
15. Ishii, K. J., S. Koyama, A. Nakagawa, C. Coban, and S. Akira. 2008. Host innate immune receptors and beyond: making sense of microbial infections. *Cell Host Microbes* 3: 352–363.
16. Potter, J. A., R. E. Randall, and G. L. Taylor. 2008. Crystal structure of human IPS-1/MAVS/VISA/Cardif caspase activation recruitment domain. *BMC Struct. Biol.* 8: 11.
17. Loo, Y. M., D. M. Owen, K. Li, A. K. Erickson, C. L. Johnson, P. M. Fish, D. S. Carney, T. Wang, H. Ishida, M. Yoneyama, et al. 2006. Viral and therapeutic control of IFN-β promoter stimulator 1 during hepatitis C virus infection. *Proc. Natl. Acad. Sci. USA* 103: 6001–6006.
18. Sung, M., G. M. Poon, and J. Gariepy. 2006. The importance of valency in enhancing the import and cell routing potential of protein transduction domain-containing molecules. *Biochim. Biophys. Acta* 1758: 355–363.
19. Davenport, F. M., A. V. Hennessy, F. M. Brandon, R. G. Webster, C. D. Barrett, Jr., and G. O. Lease. 1964. Comparisons of serologic and febrile responses in humans to vaccination with influenza a viruses or their hemagglutinins. *J. Lab. Clin. Med.* 63: 5–13.
20. Tanimoto, T., R. Nakatsu, I. Fuke, T. Ishikawa, M. Ishibashi, K. Yamanishi, M. Takahashi, and S. Tamura. 2005. Estimation of the neuraminidase content of influenza viruses and split-product vaccines by immunochromatography. *Vaccine* 23: 4598–4609.
21. Kawai, T., K. Takahashi, S. Sato, C. Coban, H. Kumar, H. Kato, K. J. Ishii, O. Takeuchi, and S. Akira. 2005. IPS-1, an adaptor triggering RIG-I- and Mda5-mediated type I interferon induction. *Nat. Immunol.* 6: 981–988.
22. Jounai, N., F. Takeshita, K. Kobiyama, A. Sawano, A. Miyawaki, K. Q. Xin, K. J. Ishii, T. Kawai, S. Akira, K. Suzuki, and K. Okuda. 2007. The Atg5 Atg12 conjugate associates with innate antiviral immune responses. *Proc. Natl. Acad. Sci. USA* 104: 14050–14055.
23. Takeshita, F., K. Suzuki, S. Sasaki, N. Ishii, D. M. Klinman, and K. J. Ishii. 2004. Transcriptional regulation of the human TLR9 gene. *J. Immunol.* 173: 2552–2561.
24. Takeshita, F., K. J. Ishii, K. Kobiyama, Y. Kojima, C. Coban, S. Sasaki, N. Ishii, D. M. Klinman, K. Okuda, S. Akira, and K. Suzuki. 2005. TRAF4 acts as a silencer in TLR-mediated signaling through the association with TRAF6 and TRIF. *Eur. J. Immunol.* 35: 2477–2485.
25. Takeshita, F., T. Tanaka, T. Matsuda, M. Tozuka, K. Kobiyama, S. Saha, K. Matsui, K. J. Ishii, C. Coban, S. Akira, et al. 2006. Toll-like receptor adaptor molecules enhance DNA-raised adaptive immune responses against influenza and tumors through activation of innate immunity. *J. Virol.* 80: 6218–6224.
26. Seth, R. B., L. Sun, C. K. Ea, and Z. J. Chen. 2005. Identification and characterization of MAVS, a mitochondrial antiviral signaling protein that activates NF-κB and IRF 3. *Cell* 122: 669–682.
27. Fitzgerald, K. A., S. M. McWhirter, K. L. Faia, D. C. Rowe, E. Latz, D. T. Golenbock, A. J. Coyle, S. M. Liao, and T. Maniatis. 2003. IKKε and TBK1 are essential components of the IRF3 signaling pathway. *Nat. Immunol.* 4: 491–496.
28. Nakajima, T., C. Uchida, S. F. Anderson, C. G. Lee, J. Hurwitz, J. D. Parvin, and M. Montminy. 1997. RNA helicase A mediates association of CBP with RNA polymerase II. *Cell* 90: 1107–1112.
29. Tetsuka, T., H. Uranishi, T. Sanda, K. Asamitsu, J. P. Yang, F. Wong-Staal, and T. Okamoto. 2004. RNA helicase A interacts with nuclear factor κB p65 and functions as a transcriptional coactivator. *Eur. J. Biochem.* 271: 3741–3751.
30. Bratt, E., and M. Ohman. 2003. Coordination of editing and splicing of glutamate receptor pre-mRNA. *RNA* 9: 309–318.
31. Maas, S., A. Rich, and K. Nishikura. 2003. A-to-I RNA editing: recent news and residual mysteries. *J. Biol. Chem.* 278: 1391–1394.
32. Lee, C. G., V. da Costa Soares, C. Newberger, K. Manova, E. Lacy, and J. Hurwitz. 1998. RNA helicase A is essential for normal gastrulation. *Proc. Natl. Acad. Sci. USA* 95: 13709–13713.
33. Soulat, D., T. Burckstummer, S. Westermayer, A. Goncalves, A. Bauch, A. Stefanovic, O. Hantschel, K. L. Bennett, T. Decker, and G. Superti-Furga. 2008. The DEAD-box helicase DDX3X is a critical component of the TANK-binding kinase 1-dependent innate immune response. *EMBO J.* 27: 2135–2146.
34. Hacker, H., H. Mischak, G. Hacker, S. Eser, N. Prenzel, A. Ullrich, and H. Wagner. 1999. Cell type-specific activation of mitogen-activated protein kinases by CpG-DNA controls interleukin-12 release from antigen-presenting cells. *EMBO J.* 18: 6973–6982.
35. Stetson, D. B., and R. Medzhitov. 2006. Recognition of cytosolic DNA activates an IRF3-dependent innate immune response. *Immunity* 24: 93–103.
36. Salh, B. 2007. c-Jun N-terminal kinases as potential therapeutic targets. *Expert Opin. Ther. Targets.* 11: 1339–1353.
37. Kanzler, H., F. J. Barrat, E. M. Hessel, and R. L. Coffman. 2007. Therapeutic targeting of innate immunity with Toll-like receptor agonists and antagonists. *Nat. Med.* 13: 552–559.
38. Schmidt, C. 2007. Clinical setbacks for Toll-like receptor 9 agonists in cancer. *Nat. Biotechnol.* 25: 825–826.

JOURNAL OF BACTERIOLOGY, May 2009, p. 3321–3327 Vol. 191, No. 10
0021-9193/09/$08.00+0 doi:10.1128/JB.00120-09

Whole-Genome Tiling Array Analysis of *Mycobacterium leprae* RNA Reveals High Expression of Pseudogenes and Noncoding Regions▽†

Takeshi Akama,[1] Koichi Suzuki,[1]* Kazunari Tanigawa,[1] Akira Kawashima,[1] Huhehasi Wu,[1] Noboru Nakata,[2] Yasunori Osana,[3] Yasubumi Sakakibara,[3] and Norihisa Ishii[1]

Department of Bioregulation, Leprosy Research Center, National Institute of Infectious Diseases, Tokyo, Japan[1]; Department of Microbiology, Leprosy Research Center, National Institute of Infectious Diseases, Tokyo, Japan[2]; and Department of Biosciences and Informatics, Keio University, 3-14-1 Hiyoshi, Kohoku-ku, Yokohama, Japan[3]

Received 29 January 2009/Accepted 6 March 2009

Whole-genome sequence analysis of *Mycobacterium leprae* has revealed a limited number of protein-coding genes, with half of the genome composed of pseudogenes and noncoding regions. We previously showed that some *M. leprae* pseudogenes are transcribed at high levels and that their expression levels change following infection. In order to clarify the RNA expression profile of the *M. leprae* genome, a tiling array in which overlapping 60-mer probes cover the entire 3.3-Mbp genome was designed. The array was hybridized with *M. leprae* RNA from the SHR/NCrj-*rnu* nude rat, and the results were compared to results from an open reading frame array and confirmed by reverse transcription-PCR. RNA expression was detected from genes, pseudogenes, and noncoding regions. The signal intensities obtained from noncoding regions were higher than those from pseudogenes. Expressed noncoding regions include the *M. leprae* unique repetitive sequence RLEP and other sequences without any homology to known functional noncoding RNAs. Although the biological functions of RNA transcribed from *M. leprae* pseudogenes and noncoding regions are not known, RNA expression analysis will provide insights into the bacteriological significance of the species. In addition, our study suggests that *M. leprae* will be a useful model organism for the study of the molecular mechanism underlying the creation of pseudogenes and the role of microRNAs derived from noncoding regions.

Mycobacterium leprae, the causative agent of leprosy, cannot be cultivated in vitro. Therefore, bacteriological and pathological information, such as the mechanisms of infection, parasitization, and replication, are still largely unknown. However, whole-genome sequencing has provided insight into many biological characteristics of *M. leprae* (5). The *M. leprae* genome consists of 3.3 Mbp, which is much smaller than the 4.4 Mbp of the *Mycobacterium tuberculosis* genome. *M. leprae* has 1,605 genes and 1,115 pseudogenes, while *M. tuberculosis* has 3,959 genes and only 6 pseudogenes. The number and ratio of pseudogenes in *M. leprae* are exceptionally large by comparison with the pseudogene numbers and ratios for other pathogenic and nonpathogenic bacteria and archaea (21). A feature of *M. leprae* pseudogenes is the massive fragmentation caused by many insertions of stop codons (26). The functional roles, if any, of these unique pseudogenes and noncoding regions are unknown. However, we have shown that some *M. leprae* pseudogenes are highly expressed as RNA and that their expression levels change following macrophage infection (36). In that study, a membrane-based DNA array was created utilizing a cosmid DNA library that covered >98% of the *M. leprae* genome. mRNAs purified from *M. leprae*-infected macrophages and control bacilli were enriched by cDNA subtraction and hybridized to these arrays. Southern blot analysis of the positive cosmid clones identified 12 genes that might be important for the survival and infection of *M. leprae*. Six of the 12 genes were pseudogenes.

Pseudogenes are described as functionally silent relatives of normal genes. Since they are usually eliminated from the genome, it was speculated that the number of pseudogenes correlates with the size of the genome (28). Most pseudogenes are thought to result from a transposon insertion or inactivation of one copy after a gene duplication event (7). Because they do not create functional proteins, they are also called "junk" genes. However, some pseudogenes are expressed and function to regulate the expression of other genes (14, 20).

About one-quarter of the *M. leprae* genome is composed of noncoding regions, which constitutes a much larger proportion of the genome than the noncoding regions in *M. tuberculosis*. Gene-regulatory short RNA fragments generated from noncoding regions have been found in many organisms (17). In those cases, precursor microRNAs are transcribed independently and processed into mature forms. In eukaryotes, most of the transcriptome, which includes thousands of microRNAs, consists of noncoding RNA (24). In addition, the abundance of small RNAs in *Escherichia coli* has been estimated at 1 to 2% of the number of open reading frames (ORFs) (12).

Microarrays have facilitated transcriptome analysis through the use of probes that target a large number of genes. The technique has identified unexpected gene activity in a number of areas and in some cases has served to elucidate entire microbial metabolic processes, as exemplified by caloric restriction or oxidative stress in *E. coli* (10, 30). Moreover, RNA expression profiling has been valuable in the analysis of pathogenic bacteria. Analyses of changes in RNA expression upon

* Corresponding author. Mailing address: Department of Bioregulation, Leprosy Research Center, National Institute of Infectious Diseases, 4-2-1 Aoba-cho, Higashimurayama-shi, Tokyo 189-0002, Japan. Phone: 81-42-391-8211. Fax: 81-42-394-9092. E-mail: koichis@nih.go.jp.

† Supplemental material for this article may be found at http://jb.asm.org/.

▽ Published ahead of print on 13 March 2009.

infection of host macrophages has identified genes related to oxidative stress, proliferation, and other unknown functions in *Yersinia pestis* (causative agent of plague) (42) and *Salmonella enterica* serovar Typhi (causative agent of typhoid fever) (9). DNA microarray analysis has also found genes involved in the acid stress response (2) and transcriptional hierarchy of the flagellar system (27).

Only known or predicted genes were examined in the experiments described above. Therefore, it was not possible to analyze the RNA expression of noncoding regions and potential pseudogenes that did not have the appropriate annotation. Clone-based microarrays were developed to solve this problem (29), but they were still unable to detect genome-wide RNA expression. Finally, tiling arrays have become a useful tool for the analysis of whole-genome or chromosome expression (19) and have been used to uncover several novel RNA expression patterns (15, 38). Although the genome sequence and its annotation are known, comprehensive analysis of *M. leprae* RNA expression has not been performed. The results of our previous study and the availability of tiling arrays prompted a detailed investigation of RNA expression throughout the *M. leprae* genome. In this study, tiling arrays were used to analyze comprehensive RNA expression of genes, pseudogenes, and noncoding regions in *M. leprae*.

MATERIALS AND METHODS

Bacterial strains and growth conditions. Footpads of hypertensive nude rats (SHR/NCrj-*mu*), in which the Thai-53 strain of *M. leprae* was grown, were kindly provided by Y. Yogi, Leprosy Research Center, National Institute of Infectious Diseases. *M. leprae* was isolated as previously described (40, 41). Briefly, the skin and bones were removed from the footpad tissues. The tissues were then extensively homogenized in Hanks' balanced salt solution with 0.025% Tween 80 and centrifuged at 700 × *g* and 4°C for 10 min to remove tissue debris. The supernatant was treated with 0.5% trypsin at 37°C for 1 h, followed by centrifugation at 5,000 × *g* and 4°C for 20 min. The supernatant was discarded, and the pellet was resuspended in 10 ml Hanks' balanced salt solution with 0.025% Tween 80 and 0.25 N NaOH. A further incubation at 37°C for 15 min was followed by another centrifugation, and the pellet was resuspended in 2 ml phosphate-buffered saline. Two microliters of solution was spread on a glass slide and subjected to acid-fast staining to count the number of bacilli.

RNA extraction. *M. leprae* cells (2.8×10^{11}) were suspended in 2 ml of RNA Protect bacterial reagent (Qiagen, Germantown, MD), subjected to a vortex, and incubated for 10 min at room temperature. The cells were pelleted and resuspended in 2 ml of RNA Protect bacterial reagent, 0.4 ml of 1.0-mm zirconia beads (BioSpec Products, Bartlesville, OK), and 0.6 ml of lysis/binding buffer from the *mir*Vana miRNA isolation kit (Ambion, Austin, TX). The mixture was homogenized at 3,000 rpm for 3 min using a Micro Smash homogenizer (Tomy, Tokyo, Japan) followed by four freeze-thaw cycles. RNA was then extracted according to the manufacturer's guidelines (Ambion) and treated with DNase I (TaKaRa, Kyoto Japan).

Preparation of labeled double-stranded DNA. Twenty micrograms of total RNA from *M. leprae* was reverse transcribed using SuperScript II (Invitrogen, Carlsbad, CA). The generated cDNA was incubated with 10 ng of RNase A (Novagen, Madison, WI) at 37°C for 10 min, phenol-chloroform extracted, and precipitated with ethanol. Cy3 labeling was performed as follows: 1 μg double-stranded cDNA was incubated for 10 min at 98°C with 1 optical-density-at-600-nm unit of Cy3–9-mer Wobble primer (TriLink Biotechnologies, San Diego, CA). The addition of 8 mmol of deoxynucleoside triphosphates and 100 U of Klenow fragment (New England Biolabs, Ipswich, MA) was followed by incubation at 37°C for 2 h. The reaction was stopped by adding 0.1 volumes of 0.5 M EDTA, and the labeled cDNA was precipitated with isopropanol.

Array design. The tiling array was designed based on sequences obtained from the GenBank database (accession no. NC_002677) (5). Each probe was a 60-mer, and the adjacent probe was shifted by 18 nucleotides (a 42-nucleotide overlap). A total of 363,116 probes were designed for the sense and antisense strands and arranged on a glass plate with 22,000 control probes of randomly chosen sequences. Another array on which the probes were chosen from *M. leprae* ORFs (NimbleGen Systems, Madison, WI) was made. On this ORF array, 20 different probes were designed for each of the 1,605 ORFs. The probes were spotted onto five blocks on the glass plate, resulting in an arrangement of 160,500 probes on the ORF array.

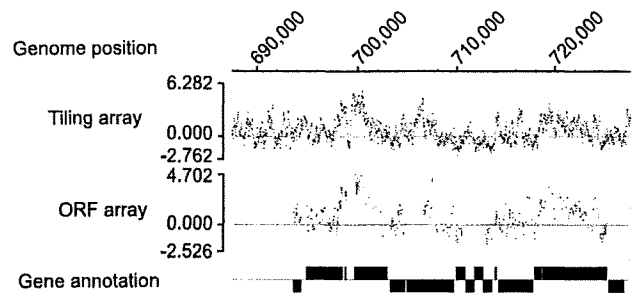

FIG. 1. Typical array data from an approximately 40-kbp region. Data from the tiling and ORF arrays are shown with the gene annotation of Cole et al. from 2001 (5) depicted as rectangles.

Hybridization and analysis of tiling and ORF arrays. Cy3-labeled samples were resuspended in 40 μl of hybridization buffer (NimbleGen Systems, Madison, WI), denatured at 95°C for 5 min, and hybridized to arrays in a MAUI hybridization system (BioMicro Systems, Salt Lake City, UT) for 18 h at 42°C. The arrays were washed using a wash buffer kit (NimbleGen Systems), dried by centrifugation, and scanned at a 5-μm resolution using the GenePix 4000B scanner (Molecular Devices, Sunnyvale, CA). NIMBLESCAN 2.3 (NimbleGen Systems) was used to obtain fluorescence intensity data from the scanned arrays.

Quantitative real-time PCR. The cDNA used for tiling array was also subjected to real-time PCR analysis. The primers were designed using GENETYX version 7 (Genetyx Corporation, Tokyo, Japan) and are listed in Table S1 in the supplemental material. Preparation of *M. leprae* genomic DNA and real-time PCRs was carried out as described previously (37) with 200 nM of each primer and 0.5 ng of cDNA or 0.2 ng of genomic DNA as a control.

RESULTS

Tiling array detected highly expressed regions in genes, pseudogenes, and noncoding regions. The 116 μg of total RNA isolated from 2.8×10^{11} *M. leprae* cells was treated with DNase I. RNA quality and quantity were evaluated with an Agilent Bioanalyzer 2100 (Agilent, Foster City, CA). The ratio of 23S rRNA to 16S rRNA was 0.83, indicating that the quality of the purified RNA was good enough to proceed with array hybridization. After hybridization and detection, the scanned row signals were normalized against the signal intensities from the control probes and converted to $\log_2$ scores with the median set at zero. The corrected intensities of all probes distributed between −2.762 and 6.282 were then calculated. When the intensities of four probes within 500 bp were higher than 60% of the maximum intensity (>3.769), the region (i.e., gene, pseudogene, or noncoding region) was considered positive. When each probe was evaluated independently, 8,658 probes (2.38%) showed >60% of the maximum intensity.

In order to confirm the specificity of the tiling array, RNA from the same sample was simultaneously hybridized with the ORF array on which multiple sequence-specific probes were designed for each gene. The positive signals detected on the ORF array were consistent with those detected on the tiling array (Fig. 1). Moreover, because the tiling array probes include ORFs in their coverage of the entire genome, it is expected that more detailed information would be obtained from them. The strongest signal was identified in the rRNA; most probes in this region showed significantly higher intensity (Fig.

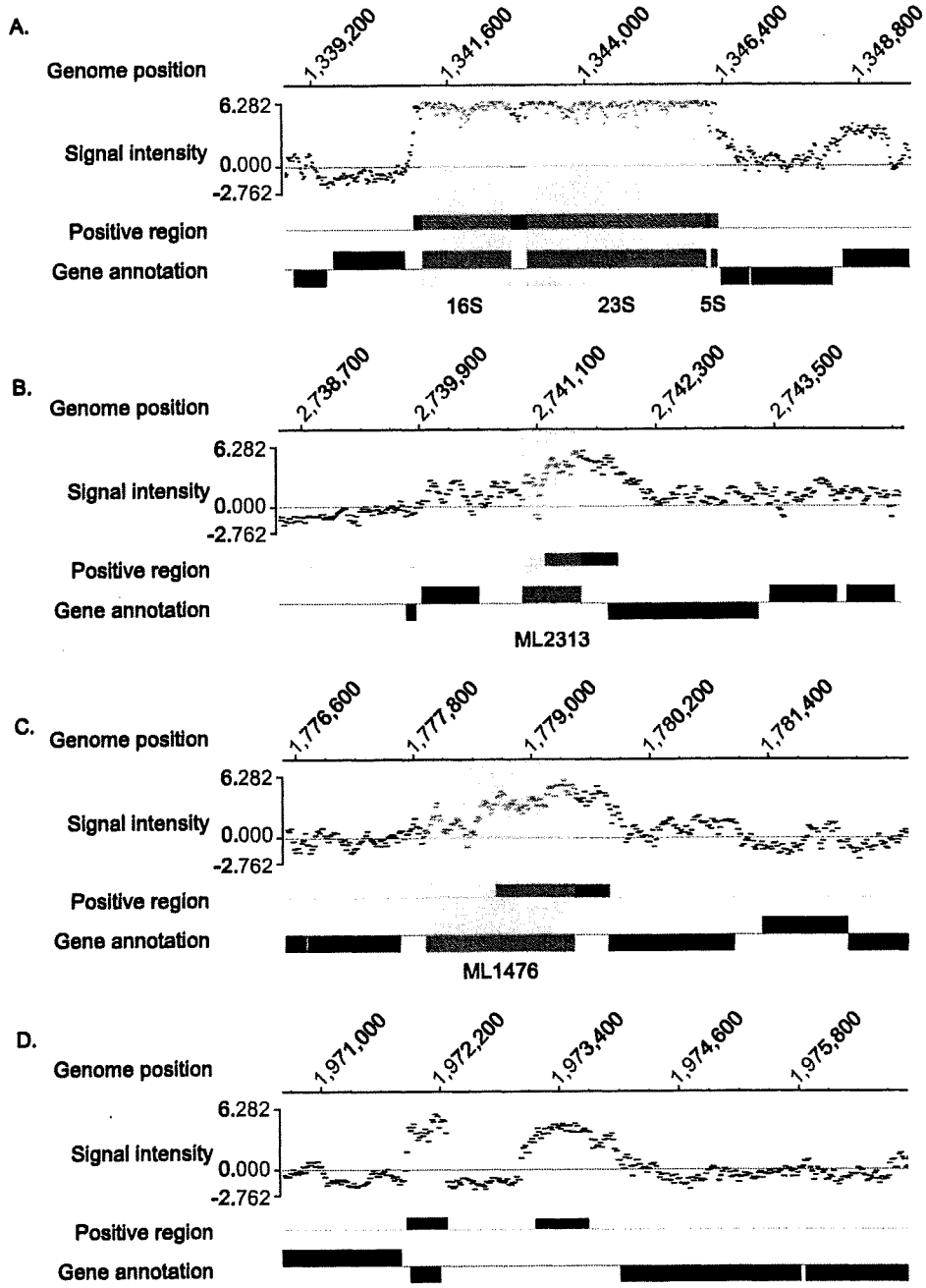

FIG. 2. Signal intensity patterns detected as highly expressed areas in the tiling array. Scanned data were normalized to $\log_2$, divided by the median, and arrayed against the corresponding *M. leprae* genome sequence. Positive areas were extracted and are depicted under the signal pattern of probes with gene and pseudogene annotations. (A) Genomic region of rRNA showing almost saturated signal intensity. (B) Highly expressed region of the gene for the hypothetical protein ML2313 (shaded area). (C) Highly expressed region of the ML1476 pseudogene (probable oxidoreductase alpha subunit; shaded area). (D) Highly expressed noncoding region in the genomic position from bp 1973155 to 1973700, which showed no homology to genes or other functional sequences by BLASTN search. Gene annotations are from reference 5.

2A). Other highly expressed areas were detected in the genes (Fig. 2B), pseudogenes (Fig. 2C), and noncoding regions (Fig. 2D). In this study, noncoding regions were defined as regions that are not annotated. rRNA and tRNA are usually considered noncoding RNA but are dealt with separately here since they are annotated in the database. An interesting feature of some highly expressed areas was that positive signals sometimes overlapped both gene/pseudogene and noncoding regions, as illustrated in Fig. 2B and C. The expression levels of each probe within a single ORF were not constant but rather quite variable, which might reflect a difference in melting temperature based on the GC content of each probe.